Viscoelastic behavior of water in the terahertz-frequency range: An inelastic x-ray scattering study

G. Monaco,[1] A. Cunsolo,[2] G. Ruocco,[3] and F. Sette[2]
[1]*Istituto Nazionale di Fisica della Materia, c/o ESRF, Boîte Postale 220, F-38043 Grenoble Cedex, France*
[2]*European Synchrotron Radiation Facility, Boîte Postale 220 F-38043 Grenoble Cedex, France*
[3]*Universitá di L'Aquila and Istituto Nazionale di Fisica della Materia, I-67100, L'Aquila, Italy*
(Received 12 April 1999)

High-resolution, inelastic x-ray scattering measurements of the dynamic structure factor $S(q,\omega)$ of liquid water in the THz frequency range have been performed as a function of wave vector q (1–7 nm^{-1}) and temperature T (273–473 K), using pressure (0–1.5 kbar) to keep the density at $\rho \approx 1$ g/cm^3. We show that, for $q \leqslant 2$ nm^{-1}, the $S(q,\omega)$ spectra can be consistently explained in terms of a hydrodynamic formalism which includes a viscoelastic, q-independent contribution to the memory function for the density fluctuations. This allows us to extract values for the infinite frequency sound velocity and for the structural relaxation time which are found to compare favorably with those obtained using techniques which probe a lower-frequency range. As a consequence, the atomic dynamics in water is shown to have a homogeneous character down to a length scale of ≈ 3 nm. At $q > 2$ nm^{-1}, we find that the viscoelastic contribution to the memory function becomes q dependent. Thus this work provides a view on the evolution of the collective dynamics of water across the q region where the continuum approximation inherent in the hydrodynamic formulation begins to fail. The physical consequences of such a result are discussed in some detail. [S1063-651X(99)03911-2]

PACS number(s): 61.20.−p, 63.50.+x, 61.10.Eq, 78.70.Ck

I. INTRODUCTION

Water has always occupied a unique role in the physics of liquids, at least for the obvious reason of its relevance to life on earth. From a very fundamental point of view, water shows peculiarities which would distinguish it from most of the other liquids and this, consequently, has attracted a lot of interest. As concerns density fluctuations in liquid water—the main subject of the present paper—their study finds considerable motivation essentially in two basic and still open issues which are suggested by the investigation of the supercooled state [1], and are recalled in the following.

The first issue is related to the discovery that, as the temperature is decreased, certain thermodynamic properties, e.g., the thermal expansion coefficient and the isothermal compressibility (and therefore also the density fluctuations), seem to diverge as though they were reaching a critical point, found to be independent of the specific considered property and very close to the homogenous nucleation temperature [1]. There are several models which attempt to account for such an enhancement of density fluctuations, and a review of the most interesting ones can be found in Ref. [1]. Unfortunately, the experimental evidence that could distinguish between these models is still inconclusive. As a general consideration, all these models emphasize the ''peculiarity'' of liquid water with respect to other liquids. Indeed, the contemporary occurrence of the hydrogen bond and the 1:1 ratio of water donor to acceptor groups strongly enhances the molecular structuring ability. However, similarities between water and silica have also been suggested [2].

The second issue, which has recently attracted a lot of interest on liquid water, refers to dynamical, rather than thermodynamic, properties and, specifically, the origin of the relaxational dynamics in the THz frequency range which is observed in the dynamic structure factor $S(q,\omega)$ as obtained either by numerical computation [3–5], or, experimentally, by measurements using different techniques. These measurements include ultrasonics (US, $\omega/2\pi \approx$ 10 KHz to 100 MHz) [6–8], Brillouin light scattering (BLS, $q \approx 10^{-2}$ nm^{-1}) [9–11], inelastic (coherent) neutron scattering (INS, $q \geqslant 3$ nm^{-1}) [12], and inelastic x-ray scattering (IXS, $q \geqslant 1$ nm^{-1}) [13,14]. Studies of the effect of a similar relaxation process on the atomic dynamics have been extensively performed on many liquids with glass forming properties [15]. In that context, this relaxation is usually referred to as structural, or α relaxation, and its characteristic time τ_M is known as the structural relaxation time. Given that the structural relaxation is a typical feature of all liquids, this second issue refers to a ''normal'' liquid behavior of water.

When considering $S(q,\omega)$ spectra, the structural relaxation is usually characterized by studying its effect on the sound waves [15]. In fact, using a spectroscopic technique which probes the atomic dynamics at the frequency $\omega/2\pi$, different responses are obtained whether ω is much higher or much lower than $1/\tau_M$: in the former case, one probes the system on such a short time scale that the atomic structure cannot rearrange itself (unrelaxed limit); in the latter case, conversely, the system structure can relax (relaxed limit). As a consequence, the speed of sound shows a characteristic dispersion with both frequency and wave vector, i.e., increases from a low value in the zero frequency (wave vector) limit to a higher value in the opposite limit. In the frequency (wave vector) range between these two limits, the relaxation process can be directly accessed, since it lies inside the probed frequency window, and its spectral parameters, e.g., τ_M, can be determined. With regard to this, the ''best sensitivity'' condition is usually defined by the relation $\omega\tau_M \approx 1$.

The characteristic time τ_M has a strong temperature dependence which parallels, in first approximation, that of the shear viscosity. While in most simple liquids, and in water as well, the viscosity at the melting point is of the order of 10^{-3} Pa s, much higher values can be reached in glass forming liquids which, owing to their often complex intermolecular potentials, easily frustrate the tendency to crystallization and thus can be supercooled and remain in the liquid state at temperatures well below the melting point, T_m. As a consequence, in these systems τ_M can be easily increased from 10^{-12} s, the typical value in the normal liquid phase, up to macroscopic values when the calorimetric glass transition temperature T_g is approached. As a matter of fact, T_g is usually defined as that temperature where $\tau_M = 10^2$ s. For glass forming systems the best sensitivity condition for traditional spectroscopies like US and BLS can be easily met by choosing the temperature appropriate to bring τ_M into the desired time range, and the structural relaxation can be directly studied, at least in some temperature range below T_m. For water, conversely, due to its low supercooling capabilities, τ_M cannot be appreciably increased above the 10^{-12} s time range, and a detailed experimental characterization of the structural relaxation is still lacking: the low-frequency techniques are very far from the best sensitivity condition, which explains the often contradictory results reported so far [6–11]; the high-frequency techniques, which in principle are the best suited for such a study, have reported up to now only partial results [12,13].

Given such a scenario, we have performed an IXS experiment aiming at the experimental determination of the $S(q,\omega)$ spectra as a function of wave number (1–7 nm^{-1}) and temperature (273–473 K), varying the pressure (0–1.5 kbar) in order to keep the density at $\rho \approx 1$ g/cm^3. The main motivation is to investigate in detail the high-frequency atomic dynamics of water, and, in particular, its dependence on both wave vector and temperature. Very recently, we have presented an analysis of these IXS spectra in terms of a quite simplified model [14]. There the aim was: (i) to show that, in the case of IXS, the condition of best sensitivity for the structural relaxation is actually met in the spanned thermodynamic range, and thus the rich phenomenology of the sound dispersion [15] can indeed be observed also in water; and (ii) to give an estimate of the structural relaxation time exploiting the reduced moduli classical analysis [15]: the obtained values of τ_M were in the 10^{-12}-s range.

In the present paper, we report an analysis of the $S(q,\omega)$ spectra of water, based on a more refined and informative hydrodynamic model which accounts for both elastic and inelastic spectral components. Using this analysis, we show that up to $q = 2$ nm^{-1} the generalized hydrodynamic formalism [16] with a *q-independent*, viscoelastic contribution to the memory function for the density fluctuations can still be consistently used. This formalism allows us to extract values for the infinite frequency sound velocity and for the structural relaxation time. Such results are discussed and found to favorably compare to literature ones obtained by means of lower frequency techniques [6–11]. Thus a consistent experimental picture of such a relaxation process is derived. Moreover, for $q > 2$ nm^{-1}, we find that it is necessary to introduce a q dependence into the viscoelastic contribution to the memory function. We show, therefore, that we are probing the atomic dynamics in the q range where the continuum description inherent in the hydrodynamic formulation begins to fail. This kind of transition had not yet been experimentally observed in any liquid system. In fact, so far, only in the case of compressed noble gases had it been possible to establish a contact with the hydrodynamic regime [17].

The paper is organized as follows. In Sec. II the IXS measurements are discussed; in particular, we briefly remind the reader about the connection between the dynamic structure factor and the IXS cross section, and then we describe the experiment in some detail. In Sec. III we present the data analysis, with some coverage of the generalized hydrodynamic formalism, and of the fitting procedures that we used to describe the experimental spectra. In Sec. IV, our results are discussed and compared to those in the literature. Finally, the paper is concluded with a summary presented in Sec. V.

II. EXPERIMENT

A. IXS cross section

The experimental method utilized to study the high-frequency dynamics of water consists in a scattering process [18], where an incident photon beam (the probe) of energy $\hbar\omega_i$, momentum $\hbar\mathbf{k}_i$, and polarization $\boldsymbol{\epsilon}_i$ is brought into interaction with a system (the target), and the photons which are scattered with an energy $\hbar\omega_f$, momentum $\hbar\mathbf{k}_f$ and polarization $\boldsymbol{\epsilon}_f$ are detected. These scattered photons carry information on the spectrum of the excitations of energy, $\hbar\omega = \hbar\omega_i - \hbar\omega_f$ and momentum, $\hbar\mathbf{q} = \hbar\mathbf{k}_i - \hbar\mathbf{k}_f$, which are created (or destroyed) in the target during the interaction. In the condition of weak interaction between probe and target, the whole scattering process can be described in the framework of the linear response theory. Here the differential scattering cross section per unit ω and unit solid angle, Ω, $\partial^2\sigma/\partial\omega\partial\Omega$, is determined by a perturbative treatment of the Hamiltonian term describing the interaction between the probe and the target. In the case of photons in the $\approx$10-keV range, in absence of resonant conditions and considering energies $\hbar\omega$ in the range of the typical acoustic phonon energies (up to $\approx$100 meV), the relevant term in the probe-target interaction Hamiltonian is due to the pure charge scattering process or Thomson term

$$H_{\mathrm{int}} = \frac{1}{2} r_o \sum_j \mathbf{A}^2(\mathbf{r}_j, t), \tag{1}$$

where $r_o = e^2/m_e c^2$ is the classical electron radius, e (m_e) is the electron charge (mass), $\mathbf{A}(\mathbf{r},t)$ is the electromagnetic field potential vector, and $\mathbf{r}_j$ is the position of the jth electron. In deriving Eq. (1) we have neglected the ''magnetic'' terms (whose order of magnitude is $\approx \hbar\omega_i/m_e c^2$ smaller than the Thomson term), the term proportional to $\nabla \cdot \mathbf{A}(\mathbf{r},t)$ (relevant in resonant conditions and vanishing in the $\omega \ll \omega_i$ limit of interest here), and the direct photon-nuclei interaction term [whose order of magnitude is m_e/m_N smaller than the photon-electron interaction term Eq. (1), where m_N is the nuclear mass]. Exploiting the Fermi golden rule and the adiabatic approximation (i.e., the factorization of the electronic and nuclear eigenstates), one obtains

$$\frac{\partial^2\sigma}{\partial\omega\partial\Omega}=r_o^2(\boldsymbol{\epsilon}_i\cdot\boldsymbol{\epsilon}_f)^2\frac{k_i}{k_f}\sum_{I_n,F_n}P_{I_n}\times\left|\langle F_n|\sum_j f_j(\mathbf{q})\exp(i\mathbf{q}\cdot\mathbf{R}_j)|I_n\rangle\right|^2\delta(\omega-\omega_f-\omega_i). \tag{2}$$

Here $\langle I_n|$ ($\langle F_n|$) are the initial (final) nuclear states; P_{I_n} represents the thermal population of the initial states, and $f_j(\mathbf{q})$ is the form factor of the jth particle whose center of mass position is $\mathbf{R}_j$. At this stage, it is possible to relate the scattering cross section to the dynamic structure factor, $S(q,\omega)$, which can be written as

$$S(q,\omega)=\sum_{I_n,F_n}P_{I_n}\times\left|\langle F_n|\sum_j\exp(i\mathbf{q}\cdot\mathbf{R}_j)|I_n\rangle\right|^2\delta(\omega-\omega_f-\omega_i). \tag{3}$$

In the simple case of a monoatomic system, $f_j(\mathbf{q})=f(q)$ being independent of the jth atom, Eq. (2) reduces to the expression

$$\frac{\partial^2\sigma}{\partial\omega\partial\Omega}=r_o^2(\boldsymbol{\epsilon}_i\cdot\boldsymbol{\epsilon}_f)^2\frac{k_i}{k_f}|f(q)|^2S(q,\omega), \tag{4}$$

and thus in this case the inelastic x-ray scattering cross section is directly proportional to $S(q,\omega)$. The same result can be generalized to the case of an isotropic molecular system whenever the internal degrees of freedom of the molecules have energies much higher than those corresponding to the collective acoustic excitations. In such a case, of course, $f_j(q)$ represents the molecular form factor of the jth molecule. In the case of a general, anisotropic monomolecular system the atomic form factor, $f_j(\mathbf{q})$ holds a dependence on the jth molecule through its orientation in space; thus we are not allowed to relate the scattering cross section to $S(q,\omega)$ directly. However, it is always possible to write $f_j(\mathbf{q})=f(q)+\delta f_j(\mathbf{q})$, where $f(q)$ represents the orientationally averaged molecular form factor and $\delta f_j(\mathbf{q})$ represents the deviation of $f_j(\mathbf{q})$ from $f(q)$. Then, assuming no orientational correlation among the molecules, the scattering cross section can be written as the sum of two terms: (i) a *coherent* contribution represented once again by Eq. (4) and which directly reflects, through the isotropic component of the form factor, the molecular center of mass dynamics; and (ii) a contribution which, through the $\delta f_j(\mathbf{q})$ term, directly connects the local fluctuations in the orientational dynamics to the molecular center of mass motions. Clearly, the ratio of the integrated intensity of contribution (ii) to the coherent one is smaller than $R=(\delta f_{\max}/f(q))^2$, where $\delta f_{\max}$ is the largest possible deviation from isotropy of the molecular form factor and can be determined from the knowledge of the distribution of the electronic charge. In the case of the water molecule, $R\approx 0.016$ at $q=7$ nm^{-1} and $R\approx 0.001$ at $q=2$ nm^{-1} [19], i.e., the electronic charge distribution is almost spherical; consequently, independently of its specific spectral form, the scattering cross section can be considered all coherent, and Eq. (4) can be directly used with a confidence higher than $\approx 2\%$ in the whole spanned q range.

B. IXS setup: ID16 at the ESRF

The experiment was carried out at the very high energy resolution IXS beamline (ID16) at the European Synchrotron Radiation Facility. The x-ray source is composed of two undulators with a magnetic period of 42 mm and a total length of 3.2 m. The utilized x-ray radiation is the one corresponding to the undulator emission on the fifth harmonic, chosen to optimize the photon flux at the energy used in the present experiment (21.748 keV). After being premonochromatized to a bandwidth of 10^{-4} by a cryogenically cooled Si(1 1 1) double crystal monochromator, the beam is backscattered by the main monochromator, consisting of a flat, symmetrically cut silicon crystal oriented along the (1 1 1) direction. The Bragg angle of the monochromator is 89.98°. The family of crystalline planes used by the monochromator has to be chosen as a compromise of resolution and output flux requirements; in the present experiment we chose to work with the Si(11 11 11) reflection, which allows an overall instrumental energy resolution of 1.6-meV full width half maximum (FWHM) and a flux of 7×10^8 photons on the sample with 200-mA current in the storage ring [20]. The monochromatized beam is then focused by a grazing incidence toroidal mirror on the sample position to a spot size of 150 (vertical) $\times$350 (horizontal) μm^2 FWHM and with a divergence of 75 (vertical) $\times$120 (horizontal) μRad^2 FWHM. The radiation scattered in the nearly forward direction is analyzed by five independent analyzer systems, mounted one next to the other with a constant angular offset at 0.5 m from the extremity of a 7-m-long arm. Such an arm is capable of rotating, in the horizontal plane, in the scattering angles range comprised between $\theta_s=0°$ and 13°. The exchanged wave number q can be accordingly varied, being $q=2k_i\sin(\theta_s/2)$. The angular offset between two neighboring analyzers corresponds to a difference of 3 nm^{-1} in exchanged momentum. Each analyzer consists of $\approx$10 000 small silicon crystals of surface size 0.7×0.7 mm^2 and 3-mm height, glued with $\approx 10''$ tolerance in their relative alignment on a spherical substrate of 6.5-m radius [20]. The analyzers operate at the same reflection as the monochromator in Rowland geometry with 1:1 magnification; each of them collects the radiation scattered at the chosen scattering angle, and focuses it onto a Peltier-cooled, Si-diode detector. The dark counts due to the electronic and environmental noise are $\approx$1 count/min. The detectors energy resolution is $\approx$400 eV. Slits in front of the analyzers set the desired momentum resolution, $\approx$0.4-nm^{-1} FWHM in the present case. The energy scans are performed by varying the monochromator temperature with respect to that of the analyzer crystals; the main monochromator and analyzer temperature is controlled with a precision of $\approx$0.2 mK. The spectrometer is described in further detail elsewhere [20].

C. Experimental details and results

Distilled and deionized water has been used to fill a $\approx$1 cm^3 stainless steel cell made of INCONEL 751. This

TABLE I. The first two columns report the temperature (T) and pressure (P) of the thermodynamic points where IXS spectra have been collected. Columns 3–5 report three corresponding thermodynamic properties to be used in our data analysis, i.e., the mass density (ρ), the adiabatic sound velocity (c_o), and the ratio of constant pressure to constant volume specific heats (γ). Column 6 reports the coefficient $D_T=\chi/\gamma$, where χ is the thermal diffusivity. The last column, finally, reports the shear viscosity (η_s). Lines 1–13 report the data corresponding to the $\rho\simeq 1$ g/cm^3 measurements; line 14, conversely, corresponds to a higher density ($\rho\simeq 1.1$ g/cm^3). The data in columns 3–7 have been obtained from Ref. [21].

T (K)	P (bar)	ρ (g/cm^3)	c_o (m/s)	γ	$D_T\times 10^3$ (cm^2/s)	η_s (cP)
273	900(7)	1.042(1)	1567(6)	1.006(1)	1.50(1)	1.67(1)
277	1.00(1)	1.000(1)	1430(20)	1.000(1)	1.35(1)	1.58(1)
300	1.00(1)	0.997(1)	1510(20)	1.012(1)	1.48(1)	0.85(1)
313	186(2)	1.000(1)	1563(7)	1.028(1)	1.59(1)	0.66(1)
328	900(30)	1.022(1)	1700(20)	1.054(2)	1.77(1)	0.53(1)
333	400(3)	1.000(1)	1627(8)	1.054(1)	1.73(1)	0.48(1)
353	690(5)	1.001(2)	1687(6)	1.083(1)	1.88(1)	0.37(1)
373	1020(20)	1.001(2)	1742(7)	1.111(1)	2.02(1)	0.31(1)
393	1360(10)	1.001(3)	1789(2)	1.137(1)	2.15(1)	0.27(1)
413	1530(10)	0.993(2)	1801(2)	1.161(1)	2.27(1)	0.23(1)
433	1500(20)	0.978(2)	1778(4)	1.188(1)	2.35(1)	0.20(1)
453	1550(50)	0.965(2)	1760(10)	1.215(2)	2.45(2)	0.185(5)
473	2000(30)	0.968(1)	1807(6)	1.227(1)	2.60(1)	0.175(5)
277	3010(30)	1.109(1)	2020(40)	1.020(1)	1.70(1)	1.59(1)

cell can be pressurized by a hand pump up to 5 kbar and heated up to 700 K. The x-ray incident and scattered beam enters and leaves the liquid sample through two single crystal diamond cylindrical windows (thickness 1 mm, diameter 2.3 mm). The distance between the two windows, i.e., the sample length along the beam, is 10 mm, comparable to the x-ray photoabsorption length of water at the considered energy. The high pressure cell has been kept in vacuum in order to minimize both temperature gradients and scattering from the air surrounding the cell itself. Temperature has been measured by a Cr-Al thermocouple in thermal contact with the main body of the cell. The cell was connected to the pressure system by a 1-m-long stainless steel capillary which ensured a good thermal insulation between the cell and the room temperature environment. The pressure was monitored with a calibrated gauge (Nova Swiss) whose precision is $\approx 1\%$.

IXS spectra have been measured at different exchanged momenta q, temperatures T, and pressures P, as reported in Table I. Here we concentrate on the q range between 1.0 and 7.0 nm^{-1}. Most of the thermodynamic points were studied at four different exchanged momenta (1.0, 2.0, 4.0, and 7.0 nm^{-1}); in a few cases a narrower grid has been used. We have performed measurements in the 273–473-K temperature region, using pressure (0–1.5 kbar) to keep the density at $\simeq 1$ g/cm^3, according to the equation of state [21]. In this way, we have spanned a large range of thermodynamic conditions, as shown in Table I, where a few thermodynamic and transport parameters [21]—relevant in the following—are also reported. Finally, we have performed a further set of measurements at a temperature of 277 K and a pressure of 3 kbar, in order to study the dependence on density of the dynamic structure factor. The pressure stability was usually better than 2%, while temperature fluctuations were less than 0.2 K.

Each spectrum has been obtained by typically averaging five scans, and the acquisition time was about 150 min for each scan. The data have been normalized to the intensity of the incident beam. The instrumental resolution functions, one for each analyzer, have been assumed to be represented by the spectrum of a plexiglass sample measured at the q corresponding to its first diffraction peak (≈ 10 nm^{-1}), and at $T=10$ K; in such conditions, in fact, the scattering is dominated by its purely elastic component. The measured resolution functions are well represented by a Lorentzian shape with a 1.6-meV FWHM.

Examples of experimental spectra ($\bigcirc$) compared to the appropriate normalized resolution functions (dotted line) are reported in Figs. 1 and 2. In the former, the evolution with both P and q of the scattered signal measured at $T=277$ K is presented; in the latter, instead, the evolution with T of the scattered signal measured at selected q values is shown. As a general consideration, all spectra show a very clear inelastic signal which definitively increases with both increasing pressure (density) or temperature. Moreover, the measured signal shows a spectral shape which, at $q=2$ nm^{-1}, closely resembles the hydrodynamic Brillouin triplet and which evolves, with increasing q, toward a structureless broad band centered at $\omega=0$.

In order to relate the measured signal with $\partial^2\sigma/\partial\omega\partial\Omega$, and thus with $S(q,\omega)$, it is necessary to take into account both the photoelectric absorption and the multiple scattering contributions. In fact, the flux $\dot{N}_1$ of photons which are collected after one scattering event in the solid angle $\Delta\Omega$ and in the frequency interval $\Delta\omega/2\pi$ can be related to the incident photon flux $\dot{N}_o$ by the expression

$$\dot{N}_1=\dot{N}_o\frac{\partial^2\sigma}{\partial\omega\partial\Omega}\Delta\Omega\Delta\omega nLe^{-\mu L}, \tag{5}$$

where n is the molecular number density, L is the longitudinal sample length, and μ is the total absorption coefficient. The contribution to the actually measured signal which comes from multiple scattering events is clearly more difficult to formalize, and depends on the details of the sample shape and the spectrometer optics. However, if $\dot{N}_2$ represents the flux of outcoming photons corresponding to two scattering events, the ratio $R_{1,2}(q)$ of the integrated (over frequency) intensity of $\dot{N}_2$ to that of $\dot{N}_1$ can be estimated for the present measurements and for the $q=0$ scattering geometry. In fact, it can be shown that an upper estimate is given by

$$R_{1,2}(q=0)\leqslant\frac{\pi hnr_o^2}{Z^2S(0)}\int_0^\pi d\theta[f^2(\theta)S(\theta)]^2\approx 0.017. \tag{6}$$

Here $Z=f(0)$ is the number of electrons of the water molecule ($Z=10$); h is the transverse optical acceptance of

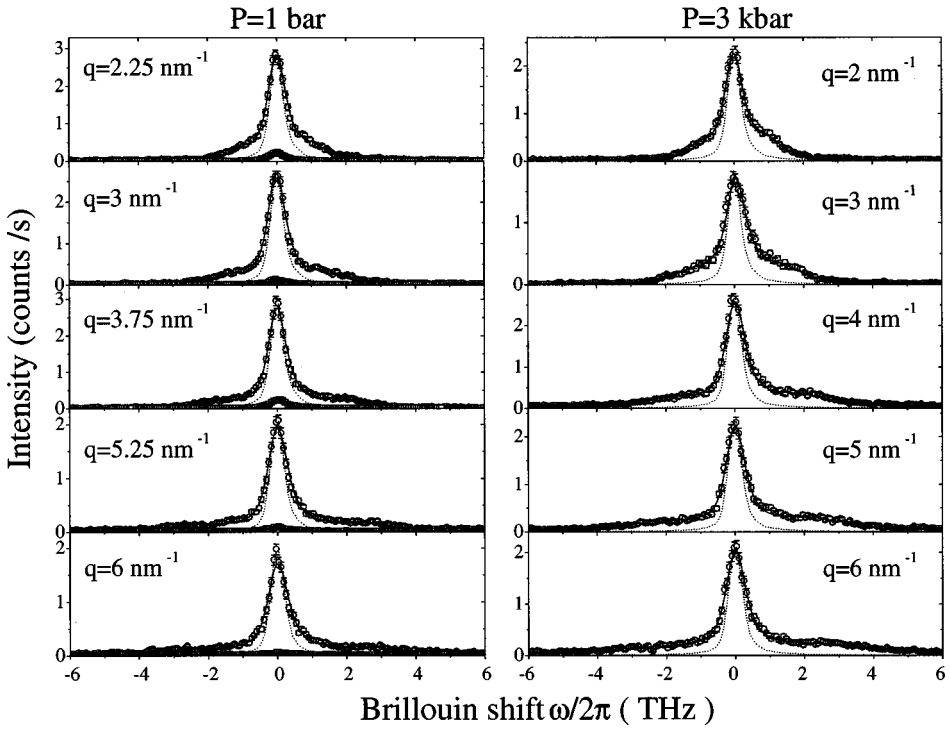

FIG. 1. Examples of the P and q dependences of the IXS spectra of liquid water (open circles) at 277 K; the data on the left hand side refer to ambient pressure ($\rho \approx 1$ g/cm^3), while those on the right hand side refer to a pressure of 3 kbar ($\rho \approx 1.1$ g/cm^3). The spectra are shown together with the fits to generalized hydrodynamics (full line), as discussed in Sec. III, and the experimental resolution function (dotted line), normalized to the intensity maximum. The measured empty cell signal (open squares), after being multiplied for the transmission of the water sample, $t = 0.48$, is compared to the spectra at ambient pressure.

the spectrometer ($h = 2$ mm); $S(\theta) = S(4\pi \sin(\theta)/\lambda)$ is the structure factor $S(q)$, evaluated at the scattering angle θ; and similarly for $f(\theta)$. To perform the calculation of relation (6) we have used $S(q)$ values taken from a molecular dynamics (MD) simulation of water ($T = 310$ K, $\rho = 1$ g/cm^3) [22], while for $f(q)$ we have used the tabulated $f(q)$ values corresponding to the F^- ion [23]. The latter choice is, once more, an upper estimate because the form factor of water is expected to decay faster than that of the F^- ion. We find that, in the $q = 0$ case, the integrated contribution coming

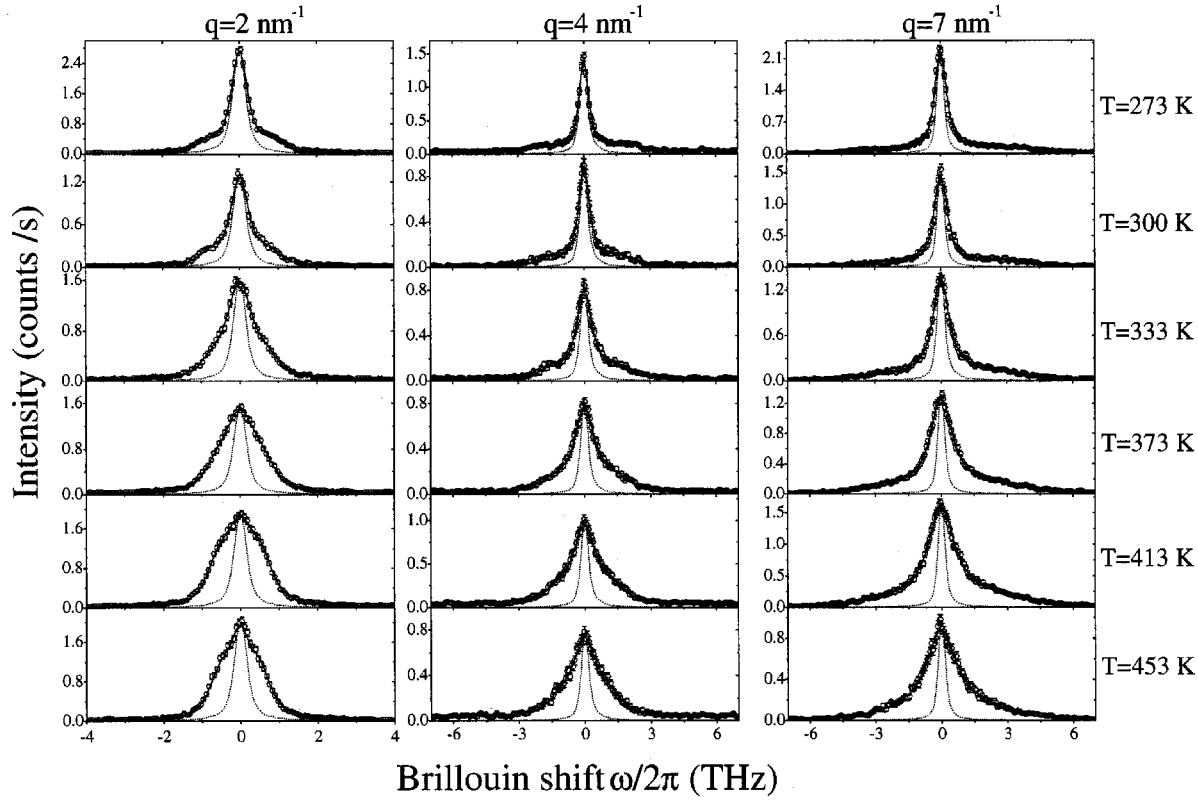

FIG. 2. Examples of the T dependence of the IXS spectra of liquid water (open circles) at the indicated temperatures and wave numbers. The data are shown together with the fits to generalized hydrodynamics (full line), as discussed in Sec. III, and the experimental resolution function (dotted line), normalized to the intensity maximum.

from two-scattering events is lower than $\approx 2\%$ of the single-scattering signal. It is worth to note that $R_{1,2}(q)$ further decreases with increasing q since, for $q>0$, the integral of the squared expression in relation (6) has to be changed into a convolution integral.

In summary, we find that the anisotropic part of the water molecule form factor and the multiple scattering contributions to the measured intensity have very different dependences on q: at low q ($q \approx 2$ nm^{-1}) we expect a maximum of $\approx 2\%$ contribution from multiple scattering, but essentially no contribution from the anisotropy in the form factor; the opposite situation holds at high q's. Thus [Eq. (5)] we can safely assume that the measured intensity is proportional to $S(q,\omega)$ with a confidence better than $\approx 2\%$.

Finally, the contribution of spurious scattering from the empty cell has been measured in all the considered scattering geometries; examples of such measurements (open squares), corrected for the transmission of the water sample ($t \approx 0.48$), are shown in Fig. 1 as compared to the total measured signal (open circles). Although this spurious signal has an integrated intensity which amounts to $\approx 5\%$ of the total signal, with almost no dependence on q, it is of negligible relevance for the results to be presented below, as will be discussed in Sec. III.

III. DATA ANALYSIS

In Sec. III A, we will recall a few general ideas of a simple formalism which is often used to describe the atomic dynamics at high frequencies and wave numbers, i.e., the so-called molecular hydrodynamics. For a complete discussion of this topic, we shall refer to well known monographs [16,17]. In Sec. III B, then, we will discuss the specific model that, within the introduced formalism, we have used to describe the measured spectra. Finally, in Sec. III C we will discuss a few relevant details on how the experimental spectra have been actually compared to the chosen model.

A. Theoretical background

We are here essentially concerned with the normalized correlation function $\Phi_q(t)$ of the density fluctuations

$$\Phi_q(t) = \frac{\langle \delta\rho_q^*(0)\,\delta\rho_q(t)\rangle}{\langle \delta\rho_q^*(0)\,\delta\rho_q(0)\rangle}, \tag{7}$$

where $\delta\rho_q(t)$ is the q component of the fluctuation of the microscopic number density $\rho(r,t)$. The dynamic structure factor $S(q,\omega)$ is then defined as

$$S(q,\omega) = S(q)\int_{-\infty}^{\infty} dt e^{-i\omega t}\Phi_q(t), \tag{8}$$

where we have introduced the static structure factor

$$S(q) = \langle \delta\rho_q^*(0)\,\delta\rho_q(0)\rangle = \frac{1}{2\pi}\int_{-\infty}^{\infty} d\omega S(q,\omega). \tag{9}$$

An equation of motion for $\Phi_q(t)$ can be written in the form of a generalized Langevin equation [16,17]

$$\frac{\partial^2\Phi_q(t)}{\partial t^2} + \omega_o^2(q)\Phi_q(t) + \int_0^t dt' m_q(t-t')\frac{\partial\Phi_q(t')}{\partial t'} = 0; \tag{10}$$

analogously, in the frequency domain, the dynamic structure factor can be written as

$$S(q,\omega) = \frac{2v_o^2q^2}{\omega}\mathrm{Im}[\omega^2 - \omega_o(q)^2 - i\omega m_q(\omega)]^{-1}, \tag{11}$$

where Im denotes the imaginary part. The parameter $\omega_o(q)$ introduced in Eqs. (10) and (11) is completely determined once one requires that the second sum rule for $S(q,\omega)$ be fulfilled, and it turns out to be

$$\omega_o^2(q) = \frac{(qv_o)^2}{S(q)}, \tag{12}$$

where v_o is the classical thermal speed which is defined in terms of the molecular mass M and the Boltzmann constant K_B as $v_o^2 = K_BT/M$. Moreover, in Eqs. (10) and (11) we have introduced the second memory function $m_q(t)$ ($m_q(\omega)$) of the so-called Zwanzig-Mori expansion of $\Phi_q(t)$ ($S(q,\omega)$) [24]. Alternatively, Eqs. (10) and (11) can be simply considered as equations which define $m_q(t)$. As a matter of fact, the real advantage of Eqs. (10) and (11) is that the introduction of simple models for $m_q(t)$—instead of directly for $\Phi_q(t)$—guarantees that at least the first two nonzero spectral moments of $S(q,\omega)$ are always respected. Clearly, at this stage [Eqs. (10) and (11)], being formal expressions, correctly describe the atomic dynamics at any time (frequency) and wave number.

According to the different kinds of dynamics which are probed, the (q,ω) space is usually divided into different regions. Two quantities can be introduced as reference points in such a space: the average intermolecular distance a and the characteristic time τ of the so-called structural relaxation. Among all the relaxations which can be active in a liquid system, and which mirror its different available dissipative processes, the structural relaxation plays a particularly important role since it is related to the cooperative processes by which the local structure, after being perturbed by an external disturbance or by a spontaneous fluctuation, rearranges toward a new equilibrium position. This relaxation is intimately related to the many-body effects which differentiate liquids from, e.g., diluted gases, and can be considered as a sort of fingerprint of the liquid state. With reference to a and τ, we can introduce two regions of the (q,ω) space which are relevant for the discussion that follows.

(i) The conditions $qa \ll 1$ and $\omega\tau \ll 1$ define the region of the (q,ω) space where simple hydrodynamics holds. In this region the fluctuations are collision dominated. Here the changes in the liquid structure induced by the density fluctuation are supposed to take place sufficiently slowly for the system to be considered in a state of local thermodynamic equilibrium. Under this condition and in the continuum limit, it is possible to obtain a closed set of equations describing the space-time variations of the conserved variables, namely, the particle number and the current and energy densities. This description becomes explicit when the values of appropriate thermodynamic derivatives and transport coefficients

are specified. The results of such calculations are available in analytical form and can be expressed by Eq. (10) with the memory function [16]

$$m_{q\to 0}(t)=\omega_o^2(q)[\gamma-1]e^{-D_T q^2 t}+2\nu_l q^2\delta(t), \qquad (13)$$

where $\gamma=C_P/C_V$ is the constant pressure to constant volume specific heat ratio; $D_T=\kappa/(\rho C_V)$, where κ is the thermal conductivity; and ν_l is the kinematic longitudinal viscosity.

(ii) If condition $\omega\tau\ll 1$ fails and $qa\sim 1$, one enters the region of so-called molecular hydrodynamics [16]. In this region the atomic dynamics is influenced both by structural and relaxational effects. For what concerns the former, their intervention directly comes into play through the structure factor $S(q)$. For what concerns the latter, instead, an appropriate viscoelastic model has to be introduced. In fact, if an external disturbance is applied to a liquid system, the observed response depends on the relative duration of the perturbation ω^{-1} as compared to the relaxation time τ. If $\omega\tau \ll 1$, the system can respond to the perturbation, and quickly takes up a new configuration; this corresponds to the simple hydrodynamic region referred to previously. If, conversely, $\omega\tau\gg 1$, the system has no time to respond before the perturbation is removed and the pre-existing equilibrium state is unchanged; in this situation the system behaves as a solid, and actually the condition $\omega\tau\gg 1$ can be used to define the purely elastic state. Measurements made in between these two time scales, i.e., in the ''relaxation region,'' enable one to determine the relaxation time.

The smooth transition from the simple hydrodynamic regime to the molecular one is the main argument used to extend the hydrodynamic description by retaining the formal structure of the equations, but replacing the thermodynamic derivatives and the transport coefficients with functions which can vary both in space (or wave number) and time (or frequency). Thus Eq. (13) can be generalized in the following way [16]:

$$m_q(t)=\omega_o^2(q)[\gamma(q)-1]e^{-D_T(q)q^2 t}+K_l(q,t), \qquad (14)$$

where $\gamma(q)$ and $D_T(q)$ are the q-dependent generalizations of the corresponding thermodynamic quantities, and $K_l(q,t)$ is directly related to the longitudinal kinematic viscosity. In fact, the requirement that Eq. (14) joins Eq. (13) in the simple hydrodynamic regime imposes the condition

$$\lim_{q\to 0}\int_0^\infty dt K_l(q,t)=q^2\nu_l. \qquad (15)$$

In addition to Eq. (15), further constraints could be imposed on $m_q(t)$ by the knowledge of higher spectral moments. However, for the sake of the present data analysis, in order to minimize the number of free parameters, it is not very useful to go beyond the second spectral moment for $S(q,\omega)$.

It has to be emphasized that the formulation presented here is a generalization of the formalism used at low q, and thus does not take into account the transverse contributions which are known to enter in the density-density dynamics of water at high q [25,4]. This latter effect can in fact be expected at q values sufficiently high such that the concept of pure transverse or longitudinal character of the modes in a liquid system begins to lose significance. In the case of water, such transverse contribution becomes definitely relevant only at q values beyond the 1–7 nm^{-1} range which will be considered here [25,4], and thus, in the following, we will simply disregard it. At this stage, in the molecular hydrodynamic approach that we just recalled here, a specific model for $m_q(t)$ has to be introduced, and this will be described in Sec. III B.

B. Choosing the model for $m_q(t)$

In the framework of Eq. (14), the simplest choice for $K_l(q,t)$ is an exponential decay. This choice, which is usually known as the *viscoelastic* model, allows for a reasonably good description of the evolution of $S(q,\omega)$ with q for $q\approx q_m$, where q_m denotes the first diffraction peak position. However, for $q\approx q_m/10$, as in our case (water has a structured first diffraction peak which approximately covers the 20–30-nm^{-1} range), the viscoelastic model begins to fail [26]. This is usually explained by saying that, when decreasing q below q_m, the memory function splits into two contributions. (i) The first one is related to molecular vibrations in the local environment, which induce a loss of correlation at the very early stages, usually on a 10^{-13}-s time scale, with almost no temperature dependence. To keep consistency with the current language used in the literature on glass forming liquids, we will refer to this contribution as to the microscopic decay [27]. (ii) The second contribution, instead, is thought to be basically due to the couplings of different q components of density fluctuations, and—as a whole—corresponds to the structural relaxation referred to previously [27]. This latter contribution is characterized by a decay time which strongly depends on temperature, changing from $\approx 10^{-12}$ s in the normal liquid phase up to about 100 s close to the glass transition temperature. As a consequence of this conceptual picture, and beginning with the MD study by Levesque *et al.* on the Lennard-Jones liquid near its triple point [28], it is customary to represent the function $K_l(q,t)$ as the sum of two exponentials. As a general result of this approach, the characteristic time of the microscopic decay turns out to be at least almost one decade in time faster than the characteristic time of the structural relaxation [28]. As a consequence, and in order to use a model with a minimum number of parameters, here we will represent the microscopic decay with a simple Markovian term. As a matter of fact, in Sec. IV this simple approximation will be shown to be detailed enough to represent our experimental data. In summary, our model for $K_l(q,t)$ reads

$$K_l(q,t)=2\gamma_o(q)\delta(t)+\frac{q^2}{\rho}\Delta^2(q)e^{-t/\tau_M(q)}, \qquad (16)$$

where $2\gamma_o(q)\delta(t)$ represents the very rapidly decaying microscopic contribution to $K_l(q,t)$, $\tau_M(q)$ is the q-dependent time which characterizes the long time tail of $K_l(q,t)$, and $\Delta^2(q)$ is the structural relaxation strength which is related to two further important quantities $c_\infty(q)$ and $c_o(q)$—the q-dependent generalizations of the usual infinite frequency and adiabatic sound speeds—as [15]

$$\Delta^2(q)=\rho[c_\infty^2(q)-c_o^2(q)]. \tag{17}$$

In fact, the second term on the right hand side of Eq. (16) is in principle able to describe the classical phenomenology of the dispersion and absorption of the sound waves, e.g., the transition of the sound speed from its low-frequency, adiabatic value, $c_o(q)$, to the high-frequency, limiting value, $c_\infty(q)$. Since we have shown in a previous study that such a transition actually occurs in liquid water at the frequencies and wave numbers probed by IXS [14], the inclusion of the exponential term in Eq. (16) to represent the structural relaxation is crucial in order to obtain reliable values for the relaxation parameters. Moreover, though in principle more rigorous and detailed expressions than a simple exponential decay could be used to represent the structural relaxation contribution [27] (as, for example, has been done in a recent analysis of depolarized light scattering spectra of water [29]), nevertheless—as we will show—we can fully account for our experimental data with a single exponential approximation, and thus there is no real need to use a more complex expression.

The first term on the right hand side of Eq. (13), corresponding to the thermal contribution, in contrast to the viscosity term (the second term on the right hand side), is characterized by a finite decay time; it is consequently more sensible to modify the $\delta(t)$ decay of the viscous term than to speculate about possible deviations of the thermal contribution from a purely exponential decay [17]. Thus we will approximate the thermal contribution with its counterpart at low q's, i.e., we will assume (i) $\omega_o(q)=\omega_o=qc_T$, where c_T is the isothermal sound velocity; (ii) $\gamma(q)=\gamma$, and (iii) $D_T(q)=D_T$. Assumption (i) is quite safe since $\omega_o^2(q) \propto [S(q)]^{-1}$ [16], and $S(q)$ is almost flat in the q range considered here ($0<q<7$ nm^{-1}). Assumption (ii) is also well verified in water in the considered q range [5]. Assumption (iii), however, is in principle quite poor since $D_T(q)$ decreases by almost a factor of 3 when q increases from its zero limit up to 7 nm^{-1} [5]. However, this is not really a relevant problem. In fact, at $q=0$, being $(q^2\Delta^2)/(\rho\omega_o^2)\approx 3$ [3,5] and being $\gamma \leqslant 1.2$ (see Table I), the strength of the thermal contribution, $\rho\omega_o^2(\gamma-1)/q^2$, is about one order of magnitude lower than that corresponding to the structural relaxation, Δ^2, and such a situation is not expected to change much when increasing q in the q range probed here. Thus, assumption (iii) simply amounts to neglect the q dependence of the characteristic time of an exponential contribution whose strength is $\approx 10\%$ of that of the structural relaxation.

In summary, to describe our experimental spectra, we will use Eq. (11) together with the Fourier transform of the following model for the memory function:

$$m_q(t)=\omega_o^2(\gamma-1)e^{-D_Tq^2t}+2\gamma_o(q)\delta(t) + \frac{q^2}{\rho}\Delta^2(q)e^{-(\omega_\infty^2(q)t)/(\omega_o^2(q)\tau_C(q))}. \tag{18}$$

In this equation, we have introduced the relaxation time $\tau_C(q)$ defined as $\tau_C(q)=\tau_M(q)[\omega_\infty^2(q)/\omega_o^2(q)]$. From a physical point of view the difference between $\tau_M(q)$ and $\tau_C(q)$ is well known [15]. The former is the characteristic time with which the long time tail of the longitudinal viscosity relaxes; see Eq. (16). In the present situation, where we assume a single exponential decay for the structural relaxation, one can show that [15] (i) $\tau_M(q)$ is also the relaxation time for the long time tail of the longitudinal modulus, $M=\rho c^2$, where c is the longitudinal speed of sound; (ii) $\tau_C(q)$ is the relaxation time for the long time tail of the longitudinal compliance, J, defined as $J=(M)^{-1}$. Moreover, in the same single exponential approximation it can also be shown that the $S(q,\omega)$ spectrum is characterized, at frequencies much lower than the Brillouin peak position and in the unrelaxed limit, by a relaxation region (mountain peak) whose characteristic time is $\tau_C(q)$ [16]. Thus $\tau_C(q)$ is the characteristic time that should in principle be compared to those obtained from analyses of other susceptibility spectra (e.g., depolarized light scattering, dielectric relaxation, etc.). Consequently, in order to facilitate such a comparison, we prefer to express Eq. (18) directly in terms of $\tau_C(q)$ instead than in terms of $\tau_M(q)$.

Finally, in concluding this subsection we want to relate the present model to the one that we used previously to analyze the inelastic x-ray scattering data, namely, the *damped harmonic oscillator model (DHO)* [30]. In fact one can see that in the limits $\gamma\approx 1$ and $\omega\tau_C(q)\gg 1$, which are both appropriate for undercooled liquids and glasses probed at the typical IXS frequencies and wave numbers, Eq. (18) reduces to

$$[m_q(t)]_{\mathrm{DHO}}=2\gamma_o(q)\delta(t)+\frac{q^2}{\rho}\Delta^2(q). \tag{19}$$

With this memory function, the dynamic structure factor [Eq. (11)] reads

$$\frac{S(q,\omega)}{S(q)}=(1-f_q)\frac{2\omega_\infty^2(q)\gamma_o(q)}{[\omega^2-\omega_\infty^2(q)]^2+[\omega\gamma_o(q)]^2}+2\pi f_q\delta(\omega), \tag{20}$$

where $\omega_\infty(q)=qc_\infty(q)$ and $f_q=1-(\omega_o(q)/\omega_\infty(q))^2$, the latter being known in the literature of glass forming systems as the nonergodicity parameter [27]. Equation (20) is exactly the expression we have used in our previous analyses of undercooled liquids and glasses [30] and also of water [14]. In the latter case, however, since both conditions $\gamma\approx 1$ and $\omega\tau_C(q)\gg 1$ are progressively violated with increasing temperature, Eq. (20) represents only a rough description of a rich phenomenology, thus motivating, in fact, the development of the more physical model given by Eq. (18).

C. Fitting procedure

In the two previous subsections, we have discussed classical models for $S(q,\omega)$. In fact, quantum effects that arise from the overlap between the single-particle wave functions can be safely neglected in the study of liquid water in the thermodynamic range of interest here. However, the quantized character of the energy transfers at a microscopic level leads to a natural imbalance of the spectral properties which is expressed by the detailed balance condition [16,17]. In order to fulfill such a requirement, we follow the common empirical prescription of multiplying the classical $S(q,\omega)$ by the factor $x(n(x)+1)$, where $x=\hbar\omega/K_BT$ and $n(x)+1$

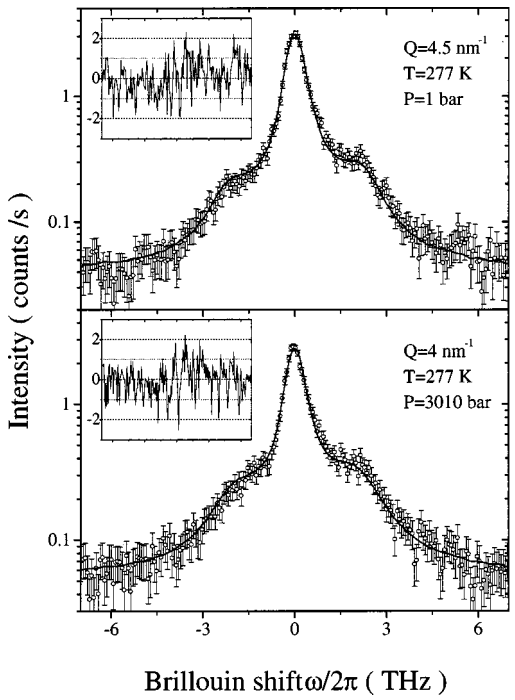

FIG. 3. Two typical examples of the measured spectra (open circles) compared to the best fits of Eq. (21) (full line). The spectra refer to the q, T, and P values indicated in the figure. A log-linear scale is used in order to emphasize the goodness of the fits. In the insets, the deviations of the fitted functions from the experimental data are reported in standard deviation units.

$=[1-\exp(-x)]^{-1}$. Thus, in order to represent the experimental spectra, we use the function

$$f(q,\omega)=[R(\omega)]\otimes[I_o(n(\omega)+1)\times \mathrm{Im}[\omega^2-\omega_o^2+i\omega m_q(\omega)]^{-1}]+B, \qquad (21)$$

where $m_q(\omega)$ is the Fourier transform of Eq. (18). In Eq. (21), $R(\omega)$ is the experimental resolution function, $\otimes$ stands for numerical convolution, I_o is an overall intensity factor, and B is an additional background term which accounts for the electronic background of the detectors and for the environmental background.

We fit Eq. (21) to the measured spectra by imposing, at each temperature, coefficients which define both the thermal diffusion term in the memory function (i.e., γ, c_T, and D_T) and the parameter ω_o. These coefficients are taken from Ref. [21] and are reported in Table I. Thus, in the fitting routine, we have five free parameters left: (i) an overall intensity factor I_o; (ii) the background term B; (iii) the strength $\Delta^2(q)$ of the structural relaxation, or, alternatively, the limiting speed $c_\infty(q)$; (iv) the compliance relaxation time $\tau_C(q)$; and, finally, (v) the instantaneous memory coefficient $\gamma_o(q)$. For the actual fitting routine, we have performed a χ^2 minimization using the standard nonlinear least squares Levenberg-Marquardt algorithm [31], with a mixed quadratic and cubic line search procedure. In all cases, the final χ^2 values have been found to be consistent with their expected values. This result can be readily appreciated looking at Fig. 3, where we report two typical examples of the measured spectra (open circles) compared to the best fitting Eq. (21) (full line).

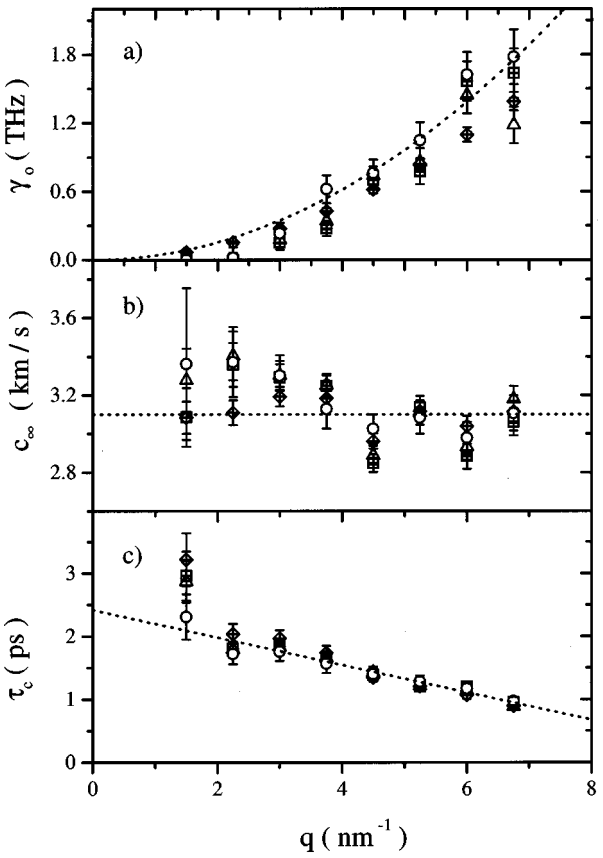

FIG. 4. The three relevant fitting parameters $\gamma_o(q)$, $c_\infty(q)$, and $\tau_C(q)$ of Eq. (21) to the set of spectra measured at $T=277$ K and $P=1$ bar as a function of q. The results corresponding to a single run of measurements (open triangles) are compared to the average results over the two runs that we have performed (open circles) and to the results obtained after having subtracted the empty cell contribution (crossed squares) from the original spectra. Moreover, the results obtained with a global fitting routine which constraints $\gamma_o(q)$ to have a q^2 dependence are reported (crossed diamonds). These parameters are all statistically consistent. The functions Eqs. (22)–(24) used to represent the q dependence of the fit parameters are also reported (dotted lines).

These examples are reported on a log-linear scale in order to better appreciate the goodness of the fits. Moreover, in the two insets of Fig. 3 we report the deviation of the fitted function from the experimental data in standard deviation units, in order to show the statistical consistency of Eq. (21) to the experimental data in the whole spanned frequency range. Further examples of Eq. (21) (full lines) best fitted to experimental data (open circles) in a large range of temperatures and wave numbers are reported in Figs. 1 and 2.

In order to assess the reliability of our rough data, and referring to Fig. 4, we discuss the results obtained for the three relevant fitting parameters $\gamma_o(q)$, $c_\infty(q)$, and $\tau_C(q)$ corresponding to the measurements performed at $T=277$ K and $P=1$ bar as a function of q. At this temperature, we have performed two different runs of measurements with slightly different sample environments. The results corresponding to a single run (open triangles) and the average results of both runs (open circles) are seen to compare reasonably well, within the estimated error bars. As a result, experimental reproducibility is guaranteed. Moreover, in or-

TABLE II. Columns 2–5 report the coefficients describing the q dependence of the fitting parameters $\gamma_o(q)$, $c_\infty(q)$, and $\tau_C(q)$ corresponding to the temperatures reported in column 1. Column 6 reports the ratio between the longitudinal kinematic viscosity, obtained as a result of the present analysis, and the shear kinematic viscosity, taken from Table I. Column 7, finally, reports the number of spectra at different q's which, at each temperature, have been found to give stable fit results. Lines 1–13 report data corresponding to the $\rho \simeq 1$ g/cm^3 measurements; line 14, conversely, corresponds to a higher density ($\rho \simeq 1.1$ g/cm^3).

T (K)	$\gamma_o \times 10^3$ (cm^2 s^{-1})	c_∞ (km s^{-1})	τ_C (ps)	ξ (nm^{-1})	ν_l/ν_s	N
273	2.92(14)	3.10(3)	4.0(8)	8.7(18)	4.8(9)	3
277	2.42(15)	3.10(4)	2.42(18)	11.1(9)	2.61(17)	8
300	2.99(18)	2.86(4)	2.4(3)	9.7(16)	4.9(6)	3
313	3.6(2)	2.73(6)	1.23(13)	12(2)	3.6(4)	3
328	3.7(2)	2.86(6)	0.76(8)	18(6)	3.5(4)	3
333	3.39(17)	2.73(5)	0.88(7)	12.9(18)	3.9(3)	3
353	2.92(18)	2.90(7)	0.70(9)	12(3)	4.3(6)	3
373	3.45(15)	2.62(5)	0.48(5)	17(4)	3.7(4)	5
393	2.87(14)	2.82(6)	0.43(3)	16(3)	4.1(3)	3
413	3.21(15)	2.61(7)	0.46(6)	10.9(19)	4.7(6)	3
433	2.51(18)	2.84(10)	0.289(7)	15.9(9)	3.9(4)	3
453	3.6(2)	2.28(12)	0.162(17)	-	3.1(4)	2
473	3.0(11)	2.6(5)	0.21(4)	-	5(3)	2
277	5.32(17)	3.30(3)	1.5(2)	50(90)	3.0(6)	5

der to check the role of the spurious scattering coming from the cell itself, in Fig. 4 we also present the results obtained after having subtracted from the spectra the empty cell contribution (corrected for the transmission of the water sample, $t=0.48$). These results (crossed squares) are once more statistically consistent with those derived neglecting the empty cell contribution (open triangles and open circles). For this reason, in the following, we will only discuss the results corresponding to the rough data, without using any additional subtraction procedure.

The stability of the best fitting parameters and the correlation coefficients among the final results have been carefully analyzed. It has been found that fitting Eq. (21) to the spectra collected at $q=1$ nm^{-1} and at all temperatures leads to strongly correlated and unstable results. For this reason, these spectra have been completely disregarded in the present analysis. For $q \geqslant 1.5$ nm^{-1} the results are generally stable and the parameters are sufficiently uncorrelated, with the exception of those corresponding to the highest temperatures ($T \geqslant 453$ K). There, in fact, due to the low speed of sound and the consequent merging of the inelastic features under the tails of the quasielastic peak, only the spectra collected at $q \geqslant 4$ nm^{-1} give reasonably safe fitting results. The number of spectra at different q's which, at each temperature, have been finally considered as meaningful for this kind of fitting analysis is reported in the last column of Table II.

IV. DISCUSSION

We will now discuss the q, T, and ρ dependences of the parameters $\gamma_o(q)$, $c_\infty(q)$, and $\tau_C(q)$, obtained as a result of the fitting procedure discussed in Sec. III C. For what concerns the other two fitting parameters, namely, I_o and B, we obtain values which are in overall agreement with our expectations based on the experimental setup. They are clearly of no relevance for the following discussion, and so they will no longer be considered here.

A. q dependence

In order to have some feeling on the reliability about the q dependence of the obtained fitting parameters, we have additionally performed *global* fits of the whole available set of experimental spectra at different q's and at a given temperature by imposing some additional constraints. As an example, in Fig. 4 we report the results obtained by imposing a q^2 dependence on $\gamma_o(q)$ (crossed diamonds). The parameters we obtain in this way are statistically consistent with the others which have been previously discussed. Similar results have been obtained by imposing a q-independent $c_\infty(q)$. From this kind of analysis some general results have been derived.

(i) The parameter $\gamma_o(q)$ shows, with increasing q, a definite increase which can be well represented by a q^2 dependence [dotted line in the Fig. 4(a)],

$$\gamma_o(q) = D_o q^2, \tag{22}$$

and this is the parametrization of $\gamma_o(q)$ that will be used in the following.

(ii) The parameter $c_\infty(q)$, conversely, can be described with a q-independent value [dotted line in Fig. 4(b)]. Actually, although a slight q dependence at the lowest q values can be noted in some local fit runs [e.g., open circles in Fig. 4(b)], we find it to be correlated with the specific q dependence of $\gamma_o(q)$ (see crossed diamonds at low q's); thus, since we represent $\gamma_o(q)$ with a simple q^2 dependence, we shall represent $c_\infty(q)$ with a q-independent value:

$$c_\infty(q) = c_\infty . \tag{23}$$

(iii) The parameter $\tau_C(q)$, finally, shows a definite decreasing trend with increasing q which is very stable against different fitting procedures. This behavior is well represented, in our limited q range, by a linear dependence [dotted line in Fig. 4(c)]:

$$\tau_C(q) = \tau_o(1 - q/\xi), \tag{24}$$

and this is the parametrization of $\tau_C(q)$ that will be used in the following. Further examples of the $\gamma_o(q)$, $c_\infty(q)$, and $\tau_C(q)$ values obtained at few selected temperatures are shown in Fig. 5, where the fits of Eqs. (22), (23), and (24) are also reported. The whole set of the D_o, c_∞, τ_o, and ξ values obtained at the investigated temperatures is reported in Table II.

From a qualitative point of view, the obtained results for the q dependence of the fitted parameters confirm those obtained in previous analyses. In fact, $\tau_C(q)$ decreases with increasing q, as has already been found in similar analyses performed by MD techniques on water [3–5] and, more in general, by both MD and INS on several systems [17]. While more sophisticated models have been proposed to describe the q dependence of $\tau_C(q)$ in order to be consistent with the

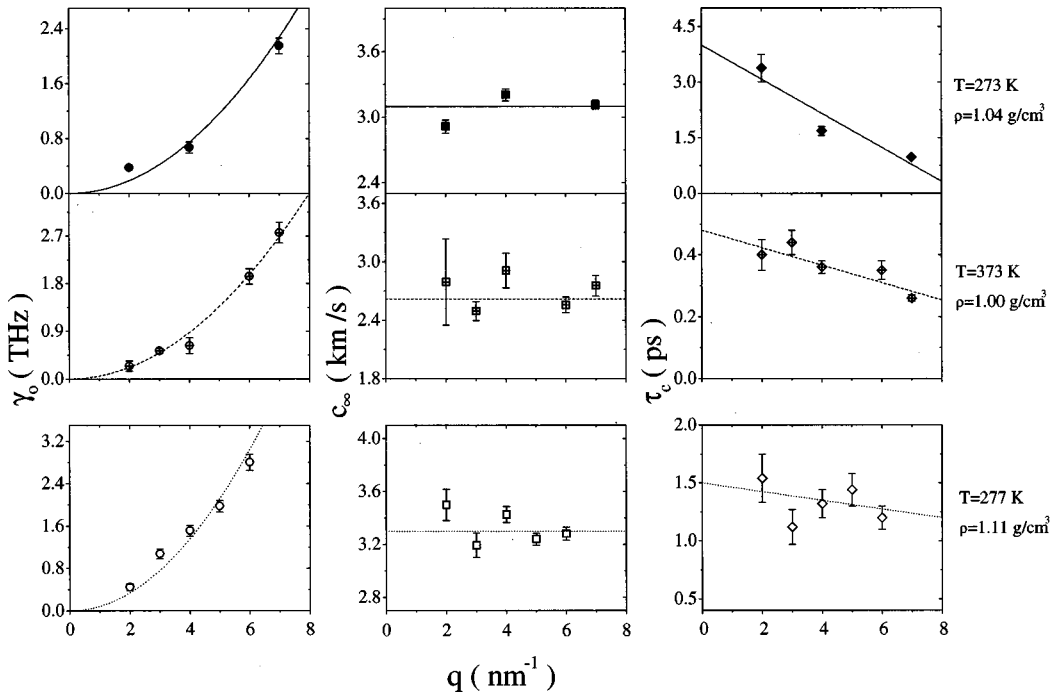

FIG. 5. Examples of the q dependence of the best fit parameters of Eqs. (18) and (21), $\gamma_o(q)$, $c_\infty(q)$, and $\tau_C(q)$, corresponding to the following thermodynamic points: $T=273$ K and $\rho\approx 1.04$ g/cm^3 (full symbols); $T=373$ K and $\rho\approx 1.00$ g/cm^3 (crossed symbols); and $T=277$ K and $\rho\approx 1.11$ g/cm^3 (open symbols). The data are shown together with the fits of Eqs. (22), (23), and (24), which are used to determine their low-q extrapolation.

very high q, single particle behavior [32], here, in the limited q range we analyze, we use the very crude linear approximation Eq. (24). In principle, it has to be expected that at lower q's, e.g., those approaching the hydrodynamic regime, $\tau_C(q)$ loses its q dependence and flattens toward a plateau. However, this is not in real contradiction with the simple linear model of Eq. (24), since the obtained ξ values are of the order of 13 nm^{-1} (see Table II), and consequently the variations predicted by Eq. (24) are practically negligible at low q's. Moreover, the value τ_o almost coincides—within the error bars—with $\tau(q=2\ \text{nm}^{-1})$. For what concerns $\gamma_o(q)$, its q^2 dependence implies that the instantaneous memory term describing the microscopic relaxation contributes quadratically in q to the linewidth of the Brillouin line. This behavior extends to liquids the similar results obtained so far in different glasses by IXS [30]; in fact, in those systems the condition $\omega\tau_C(q)\gg 1$ is very well satisfied, and so the only contribution to the Brillouin linewidth is expected to come from the very short time decay of the memory function [33].

Using the best fit parameters reported in Table II, in Fig. 6 we present the $S(q,\omega)$ [Eqs. (11) and (18)] model spectra (not convoluted to the resolution function) which correspond to the experimental data reported in Fig. 2. From an inspection of these model spectra, as compared to the experimental ones, some general conclusions can be drawn. In the data at $q=2$ nm^{-1}, an evolution with temperature is clearly visible, and it has the typical qualitative behavior expected when a relaxation is active in the explored dynamical range. Such an evolution can be described in three different steps. (i) At low temperatures, the Brillouin peaks stay in their unrelaxed position, $\omega=qc_\infty$, while the quasielastic line (mountain peak) of width $1/\tau_C$ is very narrow, given that $\omega\tau_C\gg 1$. (ii) As the temperature rises, the central line becomes broader and broader until the condition $\omega\tau_C\approx 1$ is reached, where the relaxational and propagating dynamics are on the same time scale. Under this condition, the Brillouin peaks progressively broaden to the extent that they almost disappear merging in the tails of the relaxation band (see the spectrum at 373 K). (iii) At even higher temperatures, the Brillouin peaks show up again, become more and more narrow, and shift to the fully relaxed position $\omega=qc_o$. In this same temperature range, the relaxation band has become broad enough to appear as a progressively negligible background, and its only effect is to contribute to the Brillouin linewidth through a term which, in the pure hydrodynamic limit, is proportional to the longitudinal kinematic viscosity. Under this condition, the central contribution is entirely given by the slowly relaxing thermal diffusion motions.

At q values higher than 2 nm^{-1}, the Brillouin peaks are increasingly damped, to the extent that at $q=7$ nm^{-1} they are practically indiscernible. At $q=4$ nm^{-1}, the $\omega\tau\approx 1$ condition seems to be reached only at the highest explored temperatures, so that the transition from the unrelaxed to the relaxed limit in not fully observed.

B. T dependence

Once the q dependence of the fit parameters has been assessed, an important check of consistency of our results is obtained through Eq. (15) which, within our specific model [Eq. (18)], reads

$$\lim_{q\to 0}[\gamma_o(q)/q^2+\Delta^2(q)\tau_C(q)\omega_o^2(q)/(\rho\omega_\infty^2(q))]=\nu_l. \tag{25}$$

The $q=0$ extrapolations of the fitting parameters can be

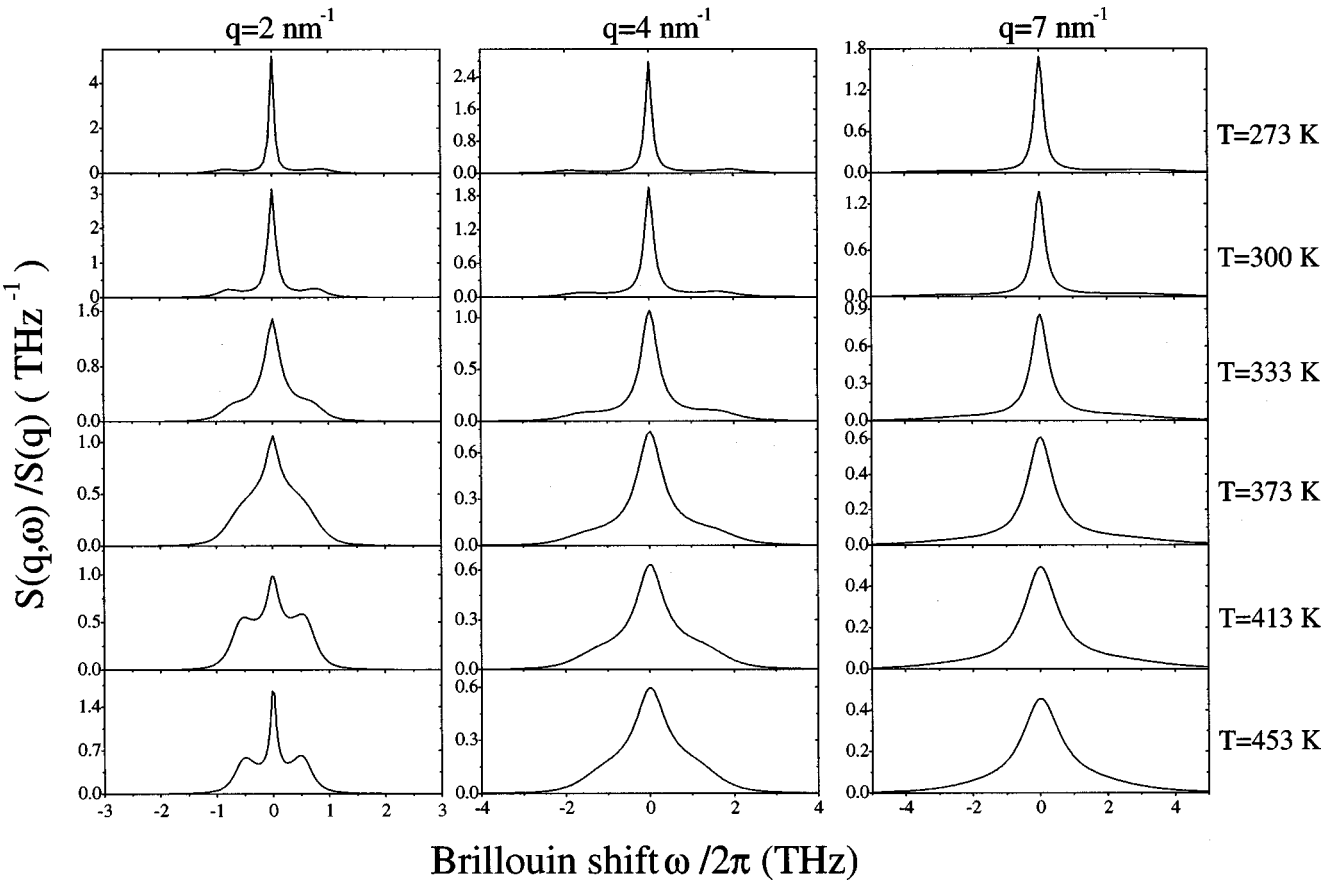

FIG. 6. The line shapes of model equations (11) and (18), which best fit the spectra reported in Fig. 2. The fit parameters used to generate this set of line shapes are reported in Table II. While at $q=2$ nm^{-1} the $\omega\tau_C\approx 1$ condition is met at $\approx$373 K, at $q=4$ nm^{-1} it seems to be met only at the highest explored temperatures, so that the fully relaxed limit is not reached. At $q=7$ nm^{-1} the Brillouin peaks are hardly discernible.

obtained through Eqs. (22)–(24). On these quantities, Eq. (25) imposes a severe constraint. Specifically the values of the longitudinal kinematic viscosity obtained via Eq. (25) from the fitting parameters derived from the IXS spectra must be compared with those obtained using other techniques. The longitudinal kinematic viscosity data ν_l (full circles for the $\rho=1$ g/cm^3 data and open circles for the $\rho=1.1$ g/cm^3 data) obtained by means of Eq. (25) from the fitting parameters reported in Table II are shown in Fig. 7(a) on a linear scale and in Fig. 7(b) on a corresponding Arrhenius plot. There are only a few other techniques which are capable of measuring ν_l; among them the most traditional ones are US (through measurements of ultrasound absorption) and BLS (through measurements of the linewidth of the Brillouin peaks). In the fully relaxed regime $\omega\tau\ll 1$, both US and BLS give ν_l values which are model independent; for water, this situation occurs at temperatures higher than $\approx$250 K for US [7,8] and $\approx$270 K for BLS [9,10]. When condition $\omega\tau\ll 1$ begins to fail, some kind of viscoelastic model has to be applied and, as in the present case, ν_l can only be obtained as a result of a fitting procedure. As far as the US measurements in water are concerned, there is a very extensive literature (see Ref. [7] for a comprehensive review). Here we will compare our results with those of Ref. [7] (crossed diamonds), since there seems to exist a general consensus on the correctness of these data [7]. The comparison between the US and our results is shown in Fig. 7, and it appears to be very good. In Fig. 7 we also report (i) the shear viscosity data (from Table I) multiplied by a factor of 4 (dotted line), which is the almost *T*- and *P*-independent ratio between the longitudinal and the shear viscosities [7]; and (ii) BLS data (down triangles) at $\rho\approx 1$ g/cm^3 [10]. The consistency between this whole body of data is once again very good. The results reported in Fig. 7 allow us to draw four important conclusions.

(i) The low-q limit of our fitting parameters correctly reproduces the longitudinal viscosity. Since the $q=0$ extrapolations of the fit parameters practically coincide with their values at $q=2$ nm^{-1}, we can conclude that at $q\leqslant 2$ nm^{-1} we are still probing a ''pure'' viscoelastic region where the dynamics is well decoupled from the structure. At larger q values, specifically in the 2–7 nm^{-1} range, one starts to probe a frequency region where the structural effects begin to enter into a description of the dynamic structure factor (molecular hydrodynamic region). Therefore, it has been possible, to bridge with continuity the hydrodynamic and the molecular hydrodynamic regions in a system at liquid densities.

(ii) The IXS spectra in the low-q region and in proximity of the maximum sensitivity region, $\omega\tau_C(T)\approx 1$, can be reliably used to obtain the longitudinal viscosity. Thus the IXS technique in this respect shows its full potentiality as a very high-frequency hypersonic technique.

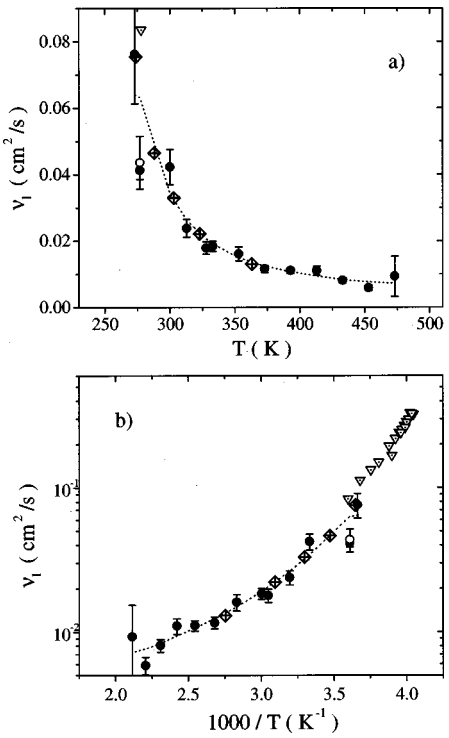

FIG. 7. T dependence of the kinematic longitudinal viscosity, ν_l, obtained from the best-fit parameters reported in Table II using Eq. (25) (full circles for the $\rho \approx 1$ g/cm^3 data and open circle for the $\rho \approx 1.1$ g/cm^3 data). The data are shown both on a linear scale (a) and on an Arrhenius plot (b). Our data are compared with US measurements at 25–50 MHz (crossed diamonds) [7], and BLS ones at ≈ 10 GHz (open squares) [10]. Both the reported US and BLS data correspond to $\rho \approx 1$ g/cm^3. Moreover, ν_s values from Table I, multiplied by a factor 4 (which is the almost T- and P-independent ratio between the longitudinal and the shear viscosity [7]), are also shown (dotted lines) in order to give an indication of the expected T dependence of ν_l. The good agreement among all the reported data can be appreciated.

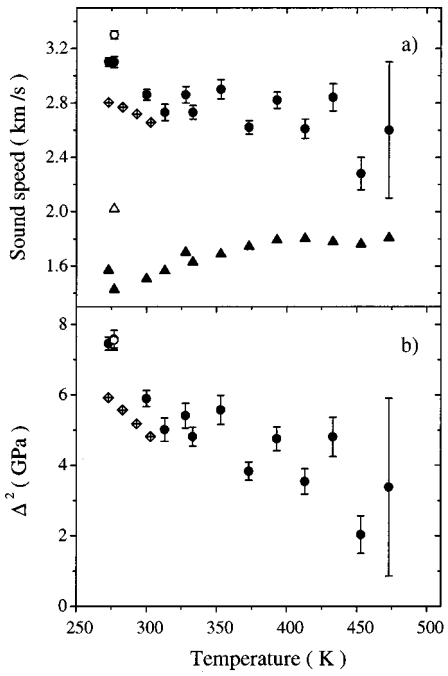

FIG. 8. T dependence of the infinite frequency sound velocity (a) and of the related structural strength (b) for our IXS data (full circles for the $\rho \approx 1$ g/cm^3 data and open circles for the $\rho \approx 1.1$ g/cm^3 data). For comparison, US results (crossed diamonds), corresponding to a density of ≈ 1 g/cm^3 [6], are also reported for both quantities. Moreover, for the sake of comparison, we also report in (a) the adiabatic speed values taken from Table I (full triangles for the $\rho \approx 1$ g/cm^3 data and open triangle for the $\rho \approx 1.1$ g/cm^3 data).

(iii) The ratio between the longitudinal and the shear kinematic viscosities appears to be constant in all of the explored conditions, thus extending to a larger thermodynamic range previous analogous observations [7]. The ν_l/ν_s ratio, obtained from our determinations of ν_l and the ν_s values of Table I [21], is reported in the last column of Table II. This ratio is 4.0 ± 0.7, and this is consistent with previous determinations [7]. It is worth remembering that the occurrence of a T-independent ν_l/ν_s ratio seems to be a prerogative of many H-bonded liquids [34].

(iv) The overall shape of ν_l shows a T dependence stronger than the Arrhenius one, resembling the Vogel-Fulcher-Tamman temperature dependence often found in glass forming liquids [15]. As a matter of fact, the stronger-than-Arrhenius T dependence of both shear and bulk viscosity in water had already been observed and interpreted either as a critical-like anomaly [11] or a typical behavior for a glass forming liquid [29]. In principle, the assumption that free volume effects influence the dynamics can also account for this characteristic behavior [35]. In this respect, the choice of keeping the density constant over the whole explored P,T region is aimed at limiting as much as possible the variation of the free volume effects. As a consequence, we can conclude that temperature influences both shear and bulk viscosities not only via free volume. Similar results were recently obtained in several glass formers [36].

At the present stage, since our model is validated by Fig. 7, we can discuss the T dependence that is obtained for the fitting parameters. The T dependence of c_∞ is reported in Fig. 8(a), while that of the corresponding strength Δ^2 is reported in Fig. 8(b) (full circles for the $\rho = 1$ g/cm^3 data, and open circles for the $\rho = 1.1$ g/cm^3 data). The values of c_∞ and of Δ^2 both decrease with increasing temperature: the first one has a value of ≈ 3150 m/s at ≈ 273 K, and decreases to ≈ 2600 m/s at high temperatures; the second one has a value of about 7.5 GPa at ≈ 273 K, and decreases to ≈ 4 GPa at high temperatures. The systematic decrease of the structural relaxation strength with increasing temperature agrees with very general considerations that ascribe the occurrence of the structural relaxation to the many-body interactions characteristic of the liquid state and which sensibly weaken when increasing the temperature. For the sake of comparison, in Fig. 8(a) we report the c_o data (full triangles for the $\rho = 1$ g/cm^3 data, and open triangles for the $\rho = 1.1$ g/cm^3 data) obtained from thermodynamics (Table I). Moreover, in Fig. 8(a) [8(b)] we also report the values (crossed diamonds) of the limiting speed (strength) obtained in an US study performed on water plus glycerol mixtures [6]. In that study, the limiting speed was measured as a function of the relative glycerol concentration, and a linear dependence was found; the values reported in Fig. 8 are the extrapolation of that trend toward the pure water case. Those data are in reason-

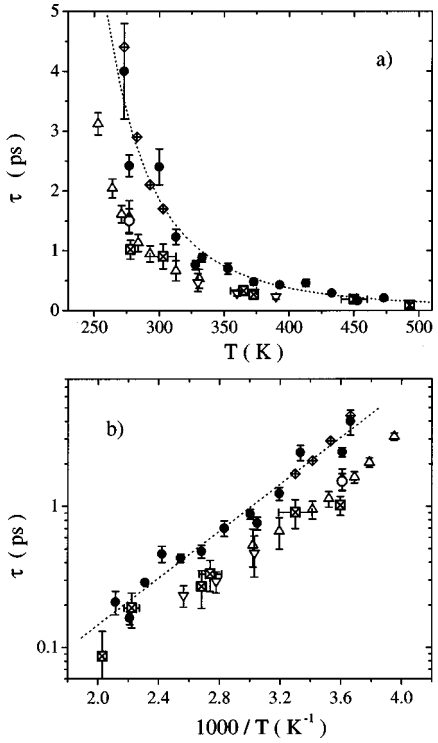

FIG. 9. T dependence of the IXS low-q extrapolations of the fitted *compliance* relaxation times, τ_C (full circles for the $\rho \approx 1$ g/cm^3 data and open circle for the $\rho \approx 1.1$ g/cm^3 data). The data are shown both on a linear scale (a) and on an Arrhenius plot (b). Our data are compared with: (i) IXS data (crossed squares) obtained from a reduced moduli analysis based on the description of the inelastic component of the IXS spectra in terms of the simple DHO model discussed in Sec. III [14]; (ii) US data (crossed diamonds) obtained from a study of water plus glycerol mixtures [6]; and (iii) DLS data which refer to the slow relaxation time which comes out in a simple description of the depolarized light scattering spectra in terms of two additive Lorentzian contributions (up triangles from Ref. [37] and down triangles from Ref. [38]). All the reported (i)–(iii) data correspond to $\rho \approx 1$ g/cm^3. In the spanned thermodynamic range, our present IXS data are well described by an Arrhenius behavior (dotted line), with an activation energy of 3.8 ± 0.6 Kcal/mol. Such a value seems actually to be common to all the reported sets of data.

able agreement with our present results. Actually, a closer inspection shows that while at ≈ 300 K the two sets of data show a complete agreement between themselves, at ≈ 273 K there are discrepancies exceeding the estimated error bars. However, the general agreement between our data and the US ones further confirms that the IXS experiment is probing the dynamical region where hydrodynamics still holds. It is worth noting that in Fig. 8 we did not report the existing BLS results for c_∞ [9,10] since they seem, at the moment, rather controversial. In fact, since the $\omega \tau_C \approx 1$ condition is never reached in BLS experiments, the obtained results are critically dependent on the model used to represent the structural relaxation. As a consequence, values varying from ≈ 3000 m/s [9] to about 2100 m/s [10] have been reported.

The T dependence of the relaxation time τ_o is reported in Fig. 9(a) on a linear scale, and in Fig. 9(b) on the corresponding Arrhenius plot (full circles for the $\rho = 1$ g/cm^3 data, and open circles for the $\rho = 1.1$ g/cm^3 data). In the thermodynamic range spanned in the present experiment, τ_o can be well described by an Arrhenius T dependence (dotted lines in Fig. 9), i.e., a temperature dependence of the form

$$\tau_o(T) = t_o e^{(E_a/K_B T)}, \tag{26}$$

with an activation energy $E_a = 3.8 \pm 0.6$ Kcal/mol, and $t_o = (3 \pm 2) \times 10^{-15}$ s.

In Figs. 9(a) and 9(b), we also report the relaxation time for the compliance obtained from the US study referred to previously [6] (crossed diamonds). The agreement between these sets of data can be easily appreciated, thus confirming once more that the present IXS measurements are actually probing the hydrodynamic properties of water. Moreover, here we present data for the hydrodynamic relaxation time τ_o, in a T range which was not previously accessible to traditional low-frequency techniques. More generally, we demonstrate the capability of IXS to give reliable values for the relaxation parameters in liquid systems at temperatures where the relaxation time is of the order of 10^{-12} s, i.e., at temperatures and frequencies which somehow represent the onset region for the ''hydrodynamic'' structural relaxation. This shows that it is now technically possible to join the traditional mechanical, US, and BLS measurements to the IXS ones in order to study the structural relaxation dynamics entering the $S(q,\omega)$ spectra in a frequency region spanning more than 14 orders of magnitude, going from the 10^2-s to the 10^{-12}-s time scale.

For the sake of comparison, in Fig. 9 we also report (i) the compliance relaxation times obtained in a recent IXS study [14] (crossed squares), and (ii) the relaxation times derived from depolarized light scattering (DLS) spectra corresponding to a density of ≈ 1 g/cm^3 (up triangles from Ref. [37], and down triangles from Ref. [38]). The data of Ref. [14] have been obtained in a simple analysis of the generalized reduced longitudinal moduli derived from the peak position of the inelastic IXS signal described by a DHO line shape; they are a factor of ≈ 2 shorter than those presented here. Since the DHO analysis corresponds to mapping the memory function with a single instantaneous process (see Sec. III), underestimated values for the relaxation times are to be expected with respect to the results of the more refined analysis presented here. However, it is remarkable that also the simple DHO analysis correctly describes the T dependence of τ_C, and gives a reasonable value for the activation energy. The DLS data refer to the ''slow'' relaxation time which comes out in a simple analysis of the DLS spectrum in terms of two additive Lorentzian processes [37,38]. In principle the DLS spectra correspond to a different correlation function from the density-density one which is of interest here. However, in Fig. 9 we report the DLS relaxation times, since it has been shown that in the case of water the DLS spectra describe the translational dynamics of the molecules through the dipole-induced-dipole induction mechanism [37–39], and that the rotational dynamics contribute to less than 10% to the total signal [37,39]. The DLS relaxation times reported in Fig. 9 show the same temperature dependence of all the other relaxation times discussed before, and are a factor of ≈ 2 shorter than those obtained here from the analysis of the $S(q,\omega)$ spectra. This is in agreement with general considerations: the DLS spectrum being a Fourier transform of a

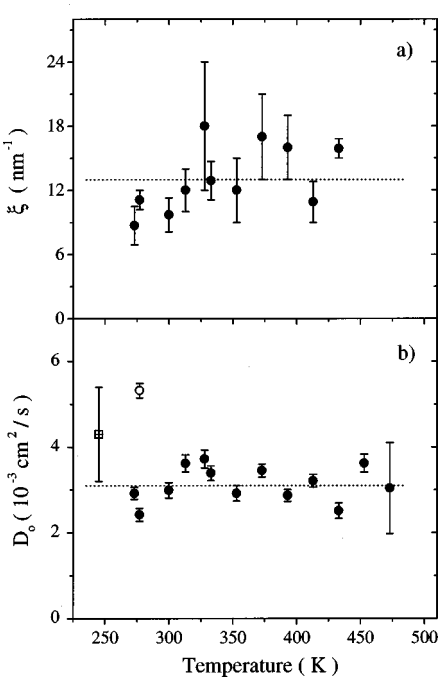

FIG. 10. (a) T dependence of the parameter ξ (full circles for the $\rho=1$ g/cm^3 data) which enters the relation (24) used to represent the q dependence of the compliance relaxation time, $\tau_C(q)$. Within the reported error bars, ξ is almost T independent (dotted line), being $\xi(T)=13\pm3$ nm^{-1}. (b) T dependence of the nonrelaxing longitudinal kinematic viscosity, $D_o(T)$ (full circles for the $\rho=1$ g/cm^3 data and open circle for the $\rho=1.1$ g/cm^3 data). Within the reported error bars, $D_o(T)$ is almost T independent (dotted line), being $D_o(T)=(3.1\pm0.4)\times10^{-3}$ cm^2/s. For the sake of comparison, we also report the D_o coefficient taken from a MD simulation of supercooled water at $T=245$ K and at $\rho=1$ g/cm^3 (square) [5]. This value has been calculated by averaging, in the 4–8-nm^{-1} q range, the almost q-independent $D_o(q)$ values obtained in Ref. [5] by using a generalized hydrodynamic model to describe the dynamic structure factor of water; the error bar associated to that value refers to the dispersion of the reported $D_o(q)$ data.

four-body correlation function, it is expected to have a characteristic decay time faster than that corresponding to the two-body, density-density, correlation function.

We observe that all the relaxation times reported in Fig. 9 are characterized by the same activation energy. In some studies [40], such an activation energy has been associated with that of the H bond, which is ≈5.5 Kcal/mol [1]. However, it seems that, rather than the local occurrence of H-bond formation and breakup, the underlying dynamical process is the structural relaxation discussed here. Clearly, this process, which is essentially cooperative in character, undoubtedly involves the H-bond network, since it is quite extended throughout the liquid in the considered thermodynamic range.

The parameter $\xi(T)$, used to represent the q dependence of $\tau_C(q)$, shows the temperature dependence reported in Fig. 10(a) (full circles for the $\rho=1$ g/cm^3 data). We can see that, within the reported error bars, ξ is almost T independent [dotted line in Fig. 10(a)], and has a value of $\xi(T)=13\pm3$ nm^{-1}. The same result holds also for the coefficient $D_o(T)$ (full circles for the $\rho=1$ g/cm^3 data and open circle for the $\rho=1.1$ g/cm^3 data), whose T dependence is reported in Fig. 10(b). In fact, in this case we can also observe that, within the reported error bars, $D_o(T)$ is almost T independent [dotted line in Fig. 10(b)], and its value is $D_o(T)=(3.1\pm0.4)\times10^{-3}$ cm^2/s. This last result compares favorably with the value recently found in the fragile glass former o-terphenyl [33]; more generally, on the basis of the IXS results, this value seems to hold for most of the liquid systems investigated up to now. For the sake of comparison, in Fig. 10(b) we also report the D_o coefficient taken from a MD simulation of supercooled water at $T=245$ K and at $\rho=1$ g/cm^3 (crossed square) [5]. This value has been calculated by averaging, in the 4–8-nm^{-1} q range, over the almost q-independent $D_o(q)$ values obtained in Ref. [5] by using a generalized hydrodynamic model to describe the dynamic structure factor of water; the error bar reported in Fig. 10(b) refers to the dispersion of the reported $D_o(q)$ data. From Fig. 10(b) we can conclude that a reasonable agreement between the MD simulation of Ref. [5] and our present results is found.

In a macroscopic picture, D_o can be considered as the residual longitudinal viscosity at infinite frequency. It should be remarked that its effect turned out to be negligible in a recent low-q, BLS study of supercooled water [10]. The results reported here, which have been obtained from the direct investigation of the high-frequency dynamics, allow us to observe, instead, a residual viscosity which, at $\rho=1$ g/cm^3, and at 273 and 473 K, respectively, accounts for $\approx5\%$ and $\approx40\%$ of the total viscosity. Given that $D_o(T)$, at low temperatures, is much smaller than the pure shear contribution, we can confirm that both shear and bulk viscosities relax in the structural relaxation process, as already proposed [10]. It is interesting to observe that the presence of a T-independent and q^2-dependent value for the nonrelaxing viscosity is a general property for a very large class of glasses at temperatures higher than ≈100 K and for frequencies up to ≈300 GHz [41]. This peculiar property is observed here to hold up to higher frequencies, and also in liquid systems.

C. ρ dependence

Finally, we will now briefly discuss the dependence on density of the quantities reported in Figs. 7–10 (full circles for the $\rho=1$ g/cm^3 data, and open circles for the $\rho=1.1$ g/cm^3 data); since we have data at only two different densities and at one temperature ($T=277$ K), our considerations, at the present stage, shall only be considered as indicative.

The effect of different densities at $T=277$ K on the total viscosity (Fig. 7) is very small. This is in agreement with previous studies [7]. At the considered temperature, in fact, it is known that the usual increase in viscosity with increasing density is compensated by the opposite effect due to the disruption of the H-bond tetrahedral network [1]. However, these competing effects differently affect the dynamics and the structure. In fact, with respect to the ambient pressure situation, (i) they increase the ability of molecules to translate and rotate [42], and thus correspondingly speed up the structural relaxation dynamics (see Fig. 9) while leaving the relaxation strength almost unchanged [see Fig. 8(b)]; and (ii) they simultaneously harden and disorder the local structure. Moreover, the increase in density is probably directly re-

sponsible for the increase of both the adiabatic and the infinite frequency sound velocities [see Fig. 8(a)]. The disruption of the H-bond tetrahedral network, instead, is probably responsible for the relevant increase of the nonrelaxing contribution to the viscosity D_o with density: D_o increases by a factor ≈ 2 when increasing ρ by $\approx 10\%$ [see Fig. 10(b)]. In fact, an increase in local disorder is generally associated to an increase of D_o [30,43].

V. CONCLUSIONS

The use of the inelastic x-ray scattering technique has allowed us to study the dynamic structure factor $S(q,\omega)$ of liquid water at $\rho \approx 1$ g/cm^3 as a function of momentum (1–7 nm^{-1}) and temperature (273–473 K). We have shown that, in the present case, the contributions of (i) rotational dynamics in the scattering cross section, and (ii) multiple scattering are both negligible with an accuracy of $\approx 2\%$. Thus, the IXS spectra can be directly assumed to represent $S(q,\omega)$ convoluted with the instrumental energy resolution function.

The $S(q,\omega)$ spectra are described using the molecular hydrodynamic formalism [16]. Such a formalism is obtained as a generalization of the usual hydrodynamic one, where the thermodynamic and transport coefficients are allowed to have both frequency and wave number dependencies in order to fulfill the first nontrivial sum rules for $S(q,\omega)$. As a matter of fact, this formalism is phenomenological in spirit since it relies on a guess for the second memory function $m_q(t)$ for the density-density correlation function. Our present guess for $m_q(t)$ is the sum of three independent contributions: (i) The first term describes the thermal diffusion process, and the usual hydrodynamic expression is directly used, with no additional momentum or frequency dependencies. Physical insight and numerical evidence are used to justify this choice. (ii) The second term describes the microscopic dynamics, and is approximated here by a Markovian memory contribution. (iii) The third term, finally, describes the structural relaxation process in terms of the traditional Maxwell viscoelasticity guess [15], but a q dependence for the relaxation parameters is allowed for. With such a guess for $m_q(t)$, one is capable to account for the entire evolution of $S(q,\omega)$ in the whole spanned thermodynamic range.

The IXS technique is, in principle, particularly well suited to study structural relaxation in water. In fact, since the structural relaxation characteristic time τ_C is of the order of 10^{-12} s at room temperature, the maximum sensitivity condition $\omega\tau_C \approx 1$ is met in the frequency range studied by IXS. Conversely, this frequency range is very far from the one studied by traditional techniques such as Brillouin light scattering or ultrasonics. We show here that, for $q \leqslant 2$ nm^{-1}, a hydrodynamic description with q-independent thermodynamic and transport coefficients can consistently be used. This is demonstrated by Fig. 7, where we show that the formalism used here allows us to derive from the IXS data the longitudinal kinematic viscosity ν_l. In the restricted thermodynamic range where ν_l data obtained using lower frequency techniques are available, we find good agreement with our new determinations. Moreover, we have been able to extend the ν_l data to the whole thermodynamic range spanned by the IXS experiment reported here. A relevant consequence of this result is the possibility to show that the ratio between the longitudinal and shear viscosity is almost pressure and temperature independent in the whole spanned thermodynamic range. Its value is $\nu_l/\nu_s = 4.0 \pm 0.7$, consistently with previous results [7]. We also obtain values for the relaxation parameters in the low-q, hydrodynamic range, namely, values for the infinite frequency sound velocity (or relaxation strength) (see Fig. 8) and for the structural relaxation time (see Fig. 9). These data are found to compare favorably to those obtained with lower frequency techniques in a thermodynamic range close to room conditions. Thanks to the IXS experiment, it has been possible to extend the existing data to a larger thermodynamic range which was up to now not accessible to lower frequency techniques.

The whole set of results obtained for the structural relaxation demonstrates the suitability of the viscoelastic model to describe $S(q,\omega)$ of water up to the previously unexplored THz frequency range, which can be somehow considered as the onset frequency range for the structural relaxation. In this respect, the IXS technique shows its full potential as a very high-frequency hypersonic technique: when used together with the traditional mechanical, US, and BLS techniques, it allows us to study the structural relaxation parameters entering in $S(q,\omega)$ spectrum in the whole frequency region going from 10^{-2} to 10^{12} Hz.

The analysis presented here shows that, for $q > 2$ nm^{-1}, it is necessary to introduce a q dependence of the longitudinal viscosity in order to describe the experimental spectra correctly. Such a q dependence essentially results in a q-dependent structural relaxation time. Thus with continuity we cross the q range where the continuum description inherent in the hydrodynamic formulation begins to fail. As a consequence of the present analysis, we show that the atomic dynamics related to density fluctuations in water has a homogeneous character down to a length scale of ≈ 3 nm.

The microscopic, Markovian contribution to the memory function is found to be quadratic in q and, in the spanned thermodynamic range, T independent, in agreement with previous results found in other liquids and glasses by IXS [30,33]. This is also in agreement with existing results for the attenuation of sound in glasses obtained at lower frequencies [41], thus extending these results both to the THz frequency range and to liquid systems. Moreover, we show that the effect of hydrostatic pressure results in a definite increase of this instantaneous memory contribution. This may be attributed to an increase in the local disorder resulting from the partial disruption of the H-bond network. At the same time, at room temperature, the breaking of the H bonds seems to speed up the dynamics related to the structural relaxation slightly. However, more extended measurements need to be performed, hopefully in the near future, in order to investigate the joint effect of density and temperature on the collective dynamics.

ACKNOWLEDGMENTS

We acknowledge C. Masciovecchio, A. Mermet, R. Verbeni, and I. Vogel for their help during the IXS measurements, and D. Gibson and L. Melesi (ILL, high pressure group) for their help during the construction and testing of the high pressure cell.

[1] P. G. Debenedetti, *Metastable Liquids* (Princeton University Press, Princeton, 1997), pp. 305–335; C. A. Angell, Annu. Rev. Phys. Chem. **34**, 593 (1983); in *Water: a Comprehensive Treatise*, edited by F. Franks (Plenum, New York, 1972), Vol. 7, pp. 1–81.

[2] P. H. Poole, M. Hemmati, and C. A. Angell, Phys. Rev. Lett. **79**, 2281 (1997).

[3] A. Rahman and F. H. Stillinger, Phys. Rev. A **10**, 368 (1974); M. Wojcik and E. Clementi, J. Chem. Phys. **85**, 6085 (1986); U. Balucani, G. Ruocco, A. Torcini, and R. Vallauri, Phys. Rev. E **47**, 1677 (1993); F. Sciortino and S. Sastry, J. Chem. Phys. **100**, 3881 (1994).

[4] M. Sampoli, G. Ruocco, and F. Sette, Phys. Rev. Lett. **79**, 1678 (1997).

[5] D. Bertolini and A. Tani, Phys. Rev. E **51**, 1091 (1995); **52**, 1699 (1995); **56**, 4135 (1997).

[6] W. M. Slie, A. R. Donfor, Jr., and T. A. Litovitz, J. Chem. Phys. **44**, 3712 (1966).

[7] C. M. Davis and J. Jarzynski, in *Water: a Comprehensive Treatise* (Ref. [1]), Vol. 1, pp. 443–461.

[8] E. Trinh and R. E. Apfel, J. Chem. Phys. **72**, 6731 (1980); V. A. Del Grosso and C. W. Mader, J. Acoust. Soc. Am. **52**, 1442 (1982).

[9] G. Maisano, P. Migliardo, F. Aliotta, C. Vasi, and F. Wanderlingh, Phys. Rev. Lett. **52**, 1025 (1984); G. Maisano, D. Majolino, F. Mallamace, P. Migliardo, F. Aliotta, C. Vasi, and F. Wanderlingh, Mol. Phys. **57**, 1083 (1986); S. Magazú, G. Maisano, D. Majolino, F. Mallamace, P. Migliardo, F. Aliotta, and C. Vasi, J. Phys. Chem. **93**, 942 (1989).

[10] A. Cunsolo and M. Nardone, J. Chem. Phys. **105**, 3911 (1996).

[11] J. Rouch, C. C. Lai, and S. H. Chen, J. Chem. Phys. **65**, 4016 (1976); **66**, 5031 (1977).

[12] J. Teixeira, M. C. Bellissent-Funel, S. H. Chen, and B. Dorner, Phys. Rev. Lett. **54**, 2681 (1985).

[13] F. Sette, G. Ruocco, M. Krisch, U. Bergmann, C. Masciovecchio, V. Mazzacurati, G. Signorelli, and R. Verbeni, Phys. Rev. Lett. **75**, 850 (1995); G. Ruocco, F. Sette, U. Bergmann, M. Krisch, C. Masciovecchio, V. Mazzacurati, G. Signorelli, and R. Verbeni, Nature (London) **379**, 521 (1996).

[14] A. Cunsolo, G. Ruocco, F. Sette, C. Masciovecchio, A. Mermet, G. Monaco, M. Sampoli, and R. Verbeni, Phys. Rev. Lett. **82**, 775 (1999); **82**, 2810(E) (1999).

[15] G. Harrison, *The Dynamic Properties of Supercooled Liquids* (Academic, New York, 1976).

[16] J. P. Boon and S. Yip, *Molecular Hydrodynamics* (Dover, New York, 1991).

[17] U. Balucani and M. Zoppi, *Dynamics of the Liquid State* (Clarendon Press, Oxford, 1994).

[18] W. Schulke, in *Handbook on Synchrotron Radiation*, edited by G. Brown and D. E. Moncton (Elsevier, Amsterdam, 1991), Vol. 3, pp. 565–637.

[19] M. Sampoli (private communication).

[20] C. Masciovecchio, U. Bergmann, M. Krisch, G. Ruocco, F. Sette, and R. Verbeni, Nucl. Instrum. Methods Phys. Res. B **111**, 181 (1996); *ibid.* **117**, 339 (1996); R. Verbeni, F. Sette, M. Krisch, U. Bergmann, B. Gorges, C. Halcoussis, K. Martel, C. Masciovecchi, J. F. Ribois, G. Ruocco, and H. Sinn, J. Synchrotron Radiat. **3**, 62 (1996).

[21] J. Kestin, J. V. Sengers, B. Kamgar-Parsi, and J. M. H. Levelt Sengers, J. Phys. Chem. Ref. Data **13**, 175 (1984).

[22] R. Frattini, M. A. Ricci, G. Ruocco, and M. Sampoli, J. Chem. Phys. **92**, 2540 (1990).

[23] *International Tables for X-ray Crystallography* (Kynoch Press, Birmingham, 1962).

[24] R. Zwanzig, in *Lectures in Theoretical Physics*, edited by W. Brittin (Wiley-Interscience, New York, 1961), Vol. 3, pp. 106–141; H. Mori, Prog. Theor. Phys. **33**, 423 (1965).

[25] F. Sette, G. Ruocco, M. Krisch, C. Masciovecchio, R. Verbeni, and U. Bergmann, Phys. Rev. Lett. **77**, 83 (1996).

[26] See, for example, *Dynamics of the Liquid State* (Ref. [17]), Fig. 6.2, p. 229. There $S(q,\omega)$ of liquid cesium ($T=308$ K) at $q=6\ \mathrm{nm}^{-1}$ is shown to be only badly described by a single-exponential memory function.

[27] W. Götze, in *Liquids, Freezing and the Glass Transition*, edited by J. P. Hansen, D. Levesque, and J. Zinn-Justin (North-Holland, Amsterdam, 1991), pp. 289–503.

[28] D. Levesque, L. Verlet, and J. Kürkijarvi, Phys. Rev. A **7**, 1690 (1973).

[29] A. P. Sokolov, J. Hurst, and D. Quitmann, Phys. Rev. B **51**, 12 865 (1995).

[30] F. Sette, M. Krisch, C. Masciovecchio, G. Ruocco, and G. Monaco, Science **280**, 1550 (1998), and references therein.

[31] J. J. More, in *Numerical Analysis*, edited by G. A. Watson, Lecture Notes in Mathematics Vol. 630 (Springer-Verlag, Berlin, 1977), pp. 105–116.

[32] A. Z. Akcasu and E. Daniels, Phys. Rev. A **2**, 962 (1970).

[33] G. Monaco, C. Masciovecchio, G. Ruocco, and F. Sette, Phys. Rev. Lett. **80**, 544 (1998); G. Monaco, D. Fioretto, C. Masciovecchio, G. Ruocco, and F. Sette, *ibid.* **82**, 1776 (1999).

[34] K. F. Herzfeld and T. A. Litovitz, *Absorption and Dispersion of Ultrasonic Waves* (Academic Press, London, 1965).

[35] G. Adam and J. H. Gibbs, J. Chem. Phys. **43**, 139 (1965).

[36] See, for example, G. Li, H. E. King, Jr., W. F. Oliver, C. A. Herbst, and H. Z. Cummins, Phys. Rev. Lett. **74**, 2280 (1995); A. Tölle, H. Schober, J. Wuttke, O. G. Randl, and F. Fujara, *ibid.* **80**, 2374 (1998).

[37] V. Mazzacurati, A. Nucara, M. A. Ricci, G. Ruocco, and G. Signorelli, J. Chem. Phys. **93**, 7767 (1990).

[38] A. Fontana, M. Nardone, and M. A. Ricci, J. Chem. Phys. **102**, 6975 (1995).

[39] R. Frattini, M. Sampoli, M. A. Ricci, and G. Ruocco, Chem. Phys. Lett. **141**, 297 (1987).

[40] C. J. Montrose, J. A. Bucaro, J. Marshall-Croakley, and T. A. Litovitz, J. Chem. Phys. **60**, 5025 (1974); O. Conde and J. Teixeira, J. Phys. (Paris) **44**, 525 (1983).

[41] S. Hunklinger and W. Arnold, in *Physical Acoustics*, edited by W. P. Mason and R. N. Thurston (Academic, New York, 1976), p. 155.

[42] F. Sciortino, A. Geiger, and H. E. Stanley, Phys. Rev. Lett. **65**, 3452 (1990); Nature (London) **354**, 218 (1991); J. Chem. Phys. **96**, 3857 (1992).

[43] A. Sokolov, J. Phys.: Condens. Matter **11**, A213 (1999).